TÜBİTAK

Turkish Journal of Earth Sciences

http://journals.tubitak.gov.tr/earth/

Research Article

Turkish J Earth Sci
(2021) 30: 93-115

doi:10.3906/yer-2006-25

Late Pleistocene-Holocene characteristics of the North Anatolian Fault at Adapazarı Basin: evidence from the age and geometry of the fluvial terrace staircases

Mehmet Korhan ERTURAÇ[1,2,*]

[1]Department of Geography, Faculty of Arts and Sciences, Sakarya University, Sakarya, Turkey
[2]Research, Development and Application Center, Sakarya University, Sakarya, Turkey

Received: 24.06.2020 • **Accepted/Published Online:** 15.10.2020 • **Final Version:** 15.01.2021

Abstract: The Late Pleistocene-Holocene evolution of the Adapazarı Basin was investigated using the stratigraphy, geometry, and absoluteluminescence dating of the 4-step fluvial terrace staircases of the Sakarya River. The results revealed that the fluvial cycle was primarily related to relative sea level changes of the Black Sea. The initiation of deposition and the abandonment ages of the terraces indicated relative high stands during marine isotope stage (MIS) 5a (~84–72 ka), 3 (40–30 ka), and 1 (9 ka-recent). The erosional periods in between the terrace steps reflected the response of the Sakarya River to the significantly low stands of the sea. The spatiotemporal position of the high terraces (T4 and T3) yielded an average of 0.78 ± 0.03 mm/year, and uniform and aseismic rock uplift rate for the NW part of the Anatolian Plate bounded by the North Anatolian Fault, which ruptured during the 1999 İzmit earthquake. The lower terrace (T1) was previously used to determine the horizontal slip rate of the Sapanca-Akyazı segment of the earthquake rupture and reported as 16.7 + 3.6/–2.5 mm/year. Further displacement measurements from the surfaces of T2 and T1 yielded a vertical slip rate of 1.49 ± 0.2 mm/year, calculated for the Late Holocene. Extrapolation of these 2 vertical rates to the south and north of the fault zone, in time and space, used in conjunction with the stratigraphy and geometry of the Adapazarı Basin, provided an estimation constraining the timing of the initiation of the fault to 450 ± 50 ka and the total thickness of the basin to ~1100 m.

Key words: Terrace staircases, Sakarya River, luminescence dating, North Anatolian Fault, Adapazarı Basin, uplift rate

1. Introduction

Stepped terrace sequences or terrace staircases (TSCs) are defined as remnants of the former floodplains within a fluvial system that are fossilized at different elevations above the present-day river channel (Bull, 2008; Pazzaglia, 2013). Formation of the TSCs was dependent on various factors. Climate-induced changes in the sediments and water flux formed cycles of aggradation and incision; therefore, the stratigraphy of the floodplains reflect the changes in the regional hydrological regime at various time-scales (Faust and Wolf, 2017). Floodplains are also known to adapt and form in response to major and long-term fluctuations in the global climate, such as stadial-interstadial cycles, i.e. marine isotope stages (MISs) (Vandenberghe, 2002, 2003; Lambeck et al., 2004; Gibbard and Levin, 2009; Macklin et al., 2012), and associated sea level oscillations (Schumm, 1993; Blum and Törnqvist, 2000). As a conclusion, the floodplains were formed and abandoned in response to fluctuations and variations in short-term regional or long-term global climate changes and consequent cycles of the sea level. Sustained surface uplift was necessary to elevate the abandoned floodplain during an erosional period, and thus favored the forming of the stepped morphology of strath terraces (Bridgland, 2000; Lavé and Avouac, 2001; Bridgland and Westaway, 2008; Westaway, 2012; Bridgland et al., 2017; Olszak, 2017).

Within this complicated framework, it is not an easy task to determine and separate the weight of impact of these variables of the equation. However, recent advancements in analytical measurements have enabled measurement of the precise geometry, as well as absolute dating, of individual fluvial terrace steps (e.g., Wallinga, 2002; Rixhon et al., 2017; Bonnet et al., 2019).Therefore, the study of TSCs provided valuable information on deciphering the timing,

* Correspondence: erturac@gmail.com

duration, and rates of earth processes, as well as regional/global climate and environmental changes controlling the geological evolution of a specific region (Wegmann and Pazzaglia, 2009; Zhang et al., 2018). The terrace surfaces and risers have been commonly used as paleo-geodetic markers to quantify the horizontal and vertical slip-rate determinations of active faults (i.e. Keller and Pinter, 1996; Cowgill 2007; Gold et al., 2011; Dikbaş et al., 2018; Zabcı, 2019).

The geodynamic evolution of the Anatolian plate involved a complex array of subduction, collision, slab detachment, back-arc spreading events, and escape tectonics (Şengör et al., 1985; Faccenna et al., 2006; Reilinger et al., 2006; Jolivet et al., 2013; Phillippon et al., 2014; Schildgen et al., 2014). The westward relative motion was mainly accommodated along 2 major tectonic structures, comprising the North Anatolian Fault Zone (NAFZ) and the East Anatolian Fault Zone (EAFZ), which form the northern and eastern boundaries of the Anatolian Plate, respectively (Şengör et al., 1985), in relation to the ongoing northward convergence of Africa-Arabia plates towards Eurasia (Reilinger et al., 2006) (Figure 1A). The prominent interactions are the Bitlis-Zagros subduction-collision to the east and the Hellenic subduction and rollback to the west. In this tectonic environment, the horizontal movement of the Anatolian Plate has been well-resolved by means of GPS velocity vectors, and definedas an extrusion towards the west with an accelerating horizontal velocity (~21–33 mm/year), while rotating in a counter-clockwise sense (Reilinger et al., 2006). Models for the driving mechanisms of the westward extrusion of Anatolia, with respect to Eurasia, can be outlined as: (i) the tectonic escape system caused by the postcollisional convergence of Eurasia and Arabia creating forces at its boundaries (Şengör et al. 1985); (ii) the slab pull of the Hellenic subduction (Armijo et al. 1999; Reilinger et al. 2006); or (iii) the coexistence processes related to these mechanisms. Recent studies have claimed that lithospheric deformation of the Anatolia was mainly controlled by collision-related tectonic escape and subduction along the Aegean Subduction Zone, including slab roll-back and slab-edge processes (i.e. Faccenna et al., 2006; Jolivet et al., 2013, 2015; Sümer et al., 2018).

The Sakarya River TSC in the Adapazarı Basin, NW Anatolia, is situated in such unique geodynamic settings. Herein, a 4-step TSC that was evidenced by detailed mapping and measuring of the terrace steps was presented. Absolute dating of the depositional periods using radiocarbon and luminescence methods enabled the direct and indirect determination of the variables mentioned above, and in detail, the characteristics of the NAF at the study area.

1.1. Regional geomorphology and geology

The study site was located on the northwestern border of the Anatolian Plate (Figure 1A) and situated in a high-relief morphology, formed of both the high peaks of western Pontide mountain range (Samanlı-Almacık Mountains, 1600–1830 m) and significant tectonic depressions, such as the İzmit-Sapanca-Adapazarı Corridor, Düzce, and Pamukova basins, and all members of the NASZ (Şengör et al., 2005, 2019) (Figure 1B).

The morphotectonic evolution of the region is controlled by the dextral NAFZ, which bifurcates into 2 main offshoots, where the northern NAF was ruptured successively as a result of the 1967 (Mudurnu Valley; M_w = 7.1), 1999a (İzmit, M_w = 7.4), and 1999b (Düzce, M_w = 7.2) earthquakes, and constitutes the main (most active) strand in the fault zone (Figure 1B).

The western part of the north Anatolian high topography (the Pontide Mountain Range) was recently dated to be exhumed in between the Oligocene and Miocene (~34–16 Ma) at a rate of 0.06 mm/year, determined by U/Th-He low-temperature apatite thermochronology (Sunal et al., 2019). This dataset also reported anomalous (younger) ages, which were interpreted as a result of increased thermal activity, resetting the ages to during the Early Quaternary (~2.5 Ma), marking the initiation of the second phase of tectonic activity (emplacement of the NAF). Akbayram et al. (2016) calculated the total offset of the NAFZ at the study area to 52 ± 1 km, which was a close approximation of the cumulative large-scale morphological offset of the Pontide mountain range (~70 km) of Sunal and Erturaç (2012). These cumulative offset determinations reflected the slip along the NAFZ as a whole, not just confined to the active strands of the fault zone today.

During the last century, the NAF showed remarkable seismic activity between 1939 and 1999, when the westward migrating earthquake sequence ruptured more than a 1000-km portion of the fault zone (Barka, 1996; Stein et al., 1997; Akyüz et al., 2002; Barka et al., 2002). The Mudurnu Valley Earthquake (Mw = 7.1; hereafter referred to as the 1967 earthquake), 17 August 1999 İzmit earthquake (M_w = 7.4, 1999a), and 12 November 1999 (M_w = 7.2; 1999b) were the most recent destructive events on the NAF, east of the Marmara region, which caused severe casualties and economic loss. The coseismic surface rupture extended for ~145 km and was detailed by field studies (Barka et al., 2002; Langridge et al., 2002; Emre et al., 2003) and space geodesy (Çakır et al., 2003). Tracing of the surface rupture revealed that it consisted of 5 segments separated by releasing step-overs, namely the Hersek, Karamürsel-Gölcük, İzmit-Sapanca Lake, Sapanca-Akyazı, and Karadere segments, from the west to the east, respectively (Barka et al., 2002). The Sapanca-Akyazı segment of the NAFZ northern strand (hereafter referred to as the SAS) trends N°75–85°W, and expresses a maximum displacement of

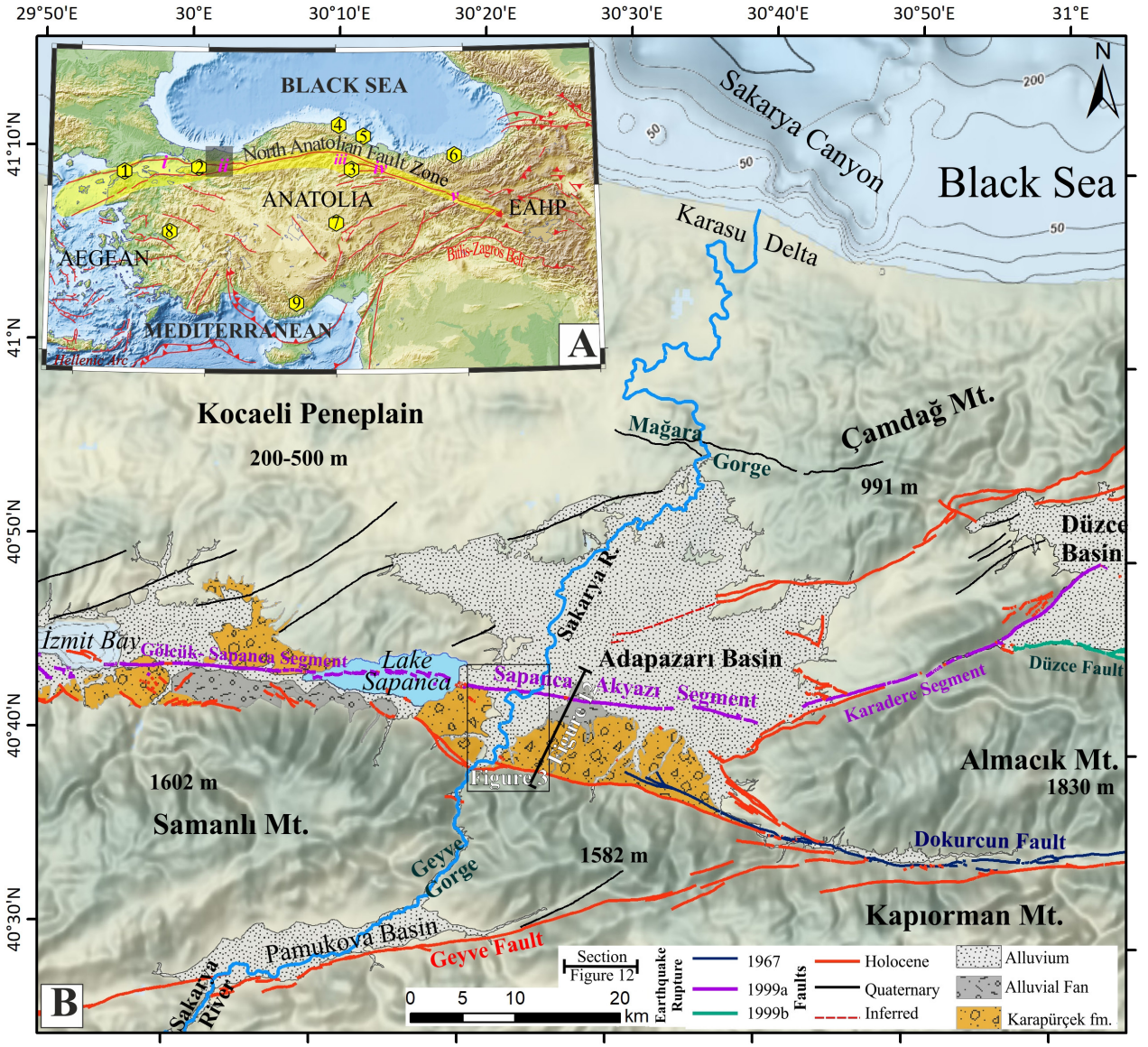

Figure 1. A) Locations of the study were with respect to the active tectonic scheme of the eastern Mediterranean, simplified after Zabcı (2019). Yellow dashed zone region marks the North Anatolian Shear Zone (NASZ; Şengör et al., 2005). Yellow polygons with numbers indicate the published U_R determinations, comprising (1) 0.27–0.72 mm/year, (2) 0.3–0.46 mm/year, (3) 0.94 ± 0.26 mm/year, (4–6) 0.2–0.3 mm/year, (7) 0.05–0.06 mm/year, (8) 0.16 mm/year, and (9) 0.6–0.7 mm/year, see text for references. Roman numerals show the position of the pull-apart basins that extinct during the middle Pleistocene, (i) Sea of Marmara (SoM); (ii) Adapazarı Basin; (iii) Suluova Basin; (iv) Niksar-Erbaa Basin; and (v) Erzincan Basin; see text for discussion. B) Broad look to the physiography of the study area. Hill-shaded topography and bathymetry are from GEBCO database. Active faults, segment names and earthquake surface ruptures were compiled from Barka et al. (2002) and Emre et al. (2018). Quaternary geological units were compiled after MTA geological maps sheets G24 (Timur and Aksay, 2002) and G25 (Gedik and Aksay, 2002). Small boxes represent the extent of Figure 3 and the profile line represents the cross-section in Figure 12.

5.2 m horizontal and 40 cm average vertical slip (Barka et al., 2002; Langridge et al., 2002), and cuts through the Adapazarı Plain. Interferometric synthetic aperture radar (INSAR) modelling of the ruptured revealed that the straight-going SAS dips 85° to the north and has a small component of normal slip (176° rake) (Çakır et al., 2003). Dikbaş et al. (2018) detailed the SAS and revealed the paleo-earthquake history for the last ~1000 years, and also constrained the Late Holocene horizontal slip rate (22 ± 3 mm/year) by measuring the cumulative offset of a lower terrace of the Sakarya River constrained by optically stimulated luminescence (OSL) dating.

1.1.1. The Adapazarı Basin

The Adapazarı Basin is a wide composite pull-apart basin that was formed by a large step-over between the Dokurcun (1967) and SAS (1999a) segments of the NAFZ (Figure 1; Neugebauer, 1995; Emre et al., 1998). It is a part of an E-W trending tectonic through the İzmit-Sapanca-Adapazarı Corridor (Emre et al., 1998; Yigitbaş et al., 2004; Gürbüz and Gürer, 2008; Tari and Tüysüz, 2016), in between the Kocaeli Peneplain to the north and the Samanlı-Kapıorman Mountains to the south. The basin has 2 prominent members, comprising the (i) Early-Middle Pleistocene Karapürçek Formation, which is a thick clastic unit that represents the first phase in the evolution of the Adapazarı Basin (Emre et al., 1998; Ünay et al., 2001) and (ii) the active depocenter (hereafter referred to as the Adapazarı Plain) which had formed on the SAS (Figure 1 B).

1.1.2. Karapürçek Formation

The Karapürçek Formation (Emre et al., 1998) is a key sedimentary unit that was deposited on the northern slopes of the Samanlı Mountain Range (Figure 1B). The formation comprises alluvial fan and fluvial sedimentary successions and its depositional environment is defined as a network of alluvial fan deposits that derived alluvium from the Samanlıdağ Mountain Range and at the latest stages, the sediments of the Sakarya River (Emre et al., 1998). The lateral equivalents of the formation are also observed to the west in between Sapanca Lake and İzmit Bay (Figure 1B). The formation has a visible thickness of more than 300 m (Emre et al., 1998). Ünay et al. (2001) detailed the rodent fauna from the formation and constrained its timing to the latest Villanyian-Biharian Mammal Ages, which correspondes to the Early-Middle Pleistocene. The deposition of the Karapürçek Formation was controlled by the present-day inactive western continuation of the Dokurcun Fault, which formed an extensional bend towards İzmit Bay, at the initial stages of the shear zone formation (Figure 1B). At the study area, the Karapürçek Formation constitutes the basement for the late Pleistocene and Holocene terraces of the Sakarya River in the Adapazarı Plain, which comprised the main scope of this study.

1.1.3. Adapazarı Plain

The Adapazarı Plain is 15 km in width and 10 km in length, and inclines smoothly towards the north at an elevation of between 50 and 30 m asl. At the active depocenter, the thickness of the alluvium has been estimated to be more than 250 m, according to the boreholes drilled by the State Hydraulic Works (Doğan, 2004) and the total Quaternary sediment thickness exceeds 1 km, which was determined via a seismic refraction survey across the basin (Karahan et al., 2001). The sedimentary fill of the plain is composed of channel fill and floodplain deposits, which reflect the fluvial cycles of the Sakarya River (Doğan, 2004). Between the Geyve Gorge and the active depocenter, the TSC of the Sakarya River sits unconformably on the Karapürçek Formation (Bilgin, 1984; Doğan, 2004; Erturaç et al., 2019a) and are observed to the south of the NAF. Recently, active aseismic subsidence was reported for the Adapazarı Plain, as evidenced with the Envisat advanced synthetic aperture radar (Hussain et al., 2016) and multitemporal Sentinel-1 data (Aslan et al., 2019), at a rate of 6–8 mm/year. Although the cause of this recent subsidence has not yet been determined, it was possibly related with draining of the former large-scale swamps within the basin in the last 50 years and accelerated usage of underground water in the last decade.

1.2. Sakarya River

The Sakarya River, which is the second largest river system in Anatolia, drains an area of 63,343 km^2, with a mean (1953–2000) discharge of 124 m^3/s, carrying ~12 million tons of suspended sediment load annually to the Black Sea (1963–1991; Öztürk, 1996). The climate of the northern part of the catchment is classified as the Marmara Transition Zone, between the Mediterranean and Black Sea climate regimes (Türkeş, 1996), with mean precipitation of 534 mm (Öztürk, 1996). The river enters the study area after passing through the narrow Geyve Gorge, which was carved inside of the Samanlı Mountain Range, connecting the Pamukova and Adapazarı Basins (Figure 1B).Through the Adapazarı Plain, the valley of the Sakarya River widens progressively within the Karapürçek Formation and exhibits a high-wavelength meandering geometry that are also reflected in meander scars (Figure 1 B). Passing through the Mağara Gorge for some 50 km, the river meets the Black Sea, forming the Karasu Delta (Görür et al., 2001; Figure 1B). Here, the continental shelf is very narrow and the effect of the sea level changes are reflected in the high relief of the Sakarya Canyon (Algan et al., 2002; Nasif et al., 2020). The age of the establishment of the river has been estimated as Early-Middle Quaternary (Emre et al., 1998) based on fluvial facies within the Karapürçek Formation.

2. Methodology

2.1. Synthetic terrace profile

Figure 2 summarizes an idealized synthetic terrace profile, which stands for a compilation of all of the terrace steps observed in the study area. On the synthetic profile, the x axis is not to scale and the y axis displays the relative elevation of the terraces above the recent floodplain. This display enabled the plotting of the maximum terrace thickness, terrace stratigraphy, sample positions, terrace types, and overall geometry of the TSC within a focus area. The numbering of the terrace steps was defined from the youngest (floodplain, T0) to the oldest, in increasing order.

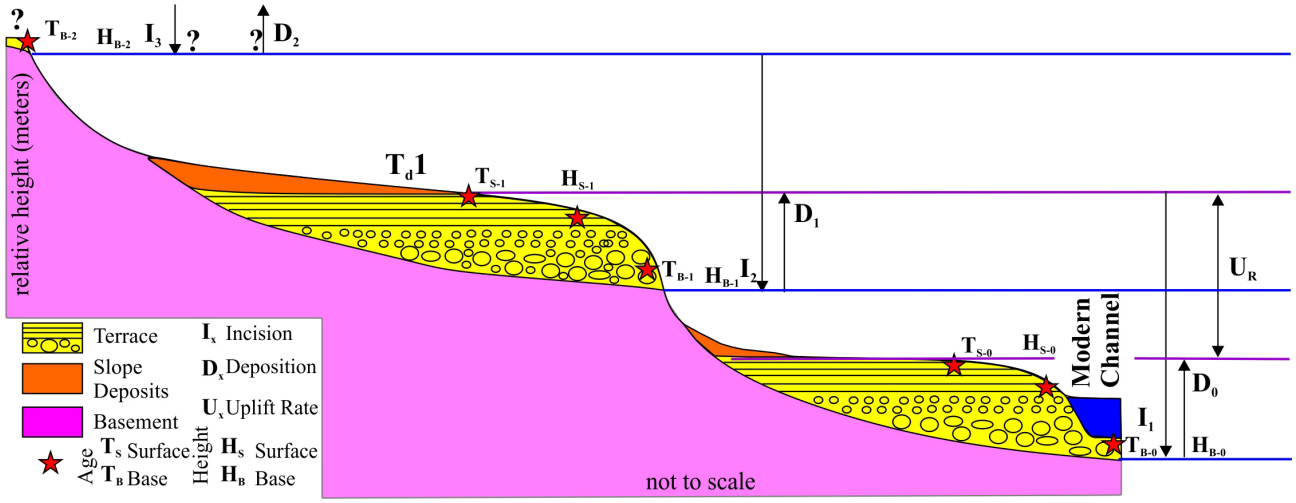

Figure 2. Schematic representation of stepped morphology of an ideal TSC and parameters used for defining the amount/rate of erosion/deposition and the rock U_R (see text for abbreviations).

Within this scheme, it was necessary to define the necessary parameters in order to utilize the terrace geometry (treads and bases) as paleo-geodetic markers that recorded the environmental changes, which enabled the calculation of the rates of process and deformation of a specific region. The terrace treads (H_{Sx}) and bases (H_{Bx}) were measured in order to determine the thickness (D) and relative elevation of the terrace tread above the floodplain (T0). The stratigraphy of the terraces should be investigated in order to discriminate possible slope deposits covering the terrace surface. Age determination, from both the base and tread (red stars in Figure 2) enabled determination of the timing of both the initiation and abandonment of the terrace development. These constraints can be further used to calculate the duration of the erosional and depositional periods, as well as the rate of incision (I_x) and deposition (D_x) in a specific time period.

The total rock uplift rate (U_R) was calculated along the river using $U_R = H_S/T_S$, where Hs is the relative elevation of the terrace riser (or strath surfaces) above the recent floodplain (m) and Ts is the achieved absolute age (ka) for the end of terrace formation prior to the initiation of the erosional period (Lambeck et al., 2004; Wegmann and Pazzaglia, 2009; Zhang et al., 2018). The uncertainty of incision rate was $\sigma_U^2 = (\sigma_{HS}/T_S)^2 + (H_S/T_s^2)^2 \sigma_{TS}^2$, where σ_{HS} is the uncertainty of the relative height of the terrace and σ_{TS} is the uncertainty of the absolute age (ka) (Zhang et al., 2018).

2.2. Mapping

Fluvial terraces perched above the active channel of the Sakarya River were mapped in the field using standard 1/25k topographic maps, 10-m resolution digital elevation models (TANDEM-X), and 1975 Keyhole images. During these surveys, the heights of the terrace treads and bedrock straths were measured toestablish the terrace stratigraphy and correlate each step. This field-based geological framework enabled the collection of meaningful luminescence and radiocarbon samples, with which it was possible to build up terrace chronology and determine the timing of key geologic events related to the evolution of the river.

The geometryof the terraces (3D positions of the strath surfaces, terrace stratigraphy, sample positions, and basal unconformities) was measured using Topcon GR-5 rtk-GPS (Topcon Positioning Systems, Inc., Livermore, CA, USA). This system utilizes 2 GPS units, comprising a base station that transmits precise position information to the mobile unit, which increases the precision to cm scale.

In order to produce a high resolution (dm scale) digital surface model (DSM) of the focus site, a low-cost and portable small unmanned aerial vehicle (sUAV) was deployed. The DJI Mavic2 Pro sUAV (DJI Science and Technology Co. Ltd., Shenzhen, China) which was equipped with a standard onboard camera and capable of shooting high resolution (5472 × 3648 pixels) still pictures, was programmed to fly along a specific route within a rectangular area at a flight altitude 150 m above the surface. The flight plan was created using Pix4D Capture (Prilly, Switzerland) as a grid flight pattern with 70% front and side overlaps of the pictures. Prior to the flights, 10 × 10 cm reflective surfaces were scattered evenly within the flight zone and each was measured using rtk-GPS to be used as ground control points for 3D correction. The captured images were processed using the structure from motion (SfM) technique, which utilized a series of 2D images to reconstruct the 3D structure of an area. SfM can produce point cloud-based 3D models, which were

processed to create high resolution orthophotos and DSMs as well. For SfM photogrammetry, the commercial Pix4D Mapper software was used. The final product, orthophoto, and DSM were reported at a 3-cm ground resolution, which later down sampled to 10 cm.

Rtk-GPS measurements and the UAV-SfM-derived DSM were also used to create high precision topographic profiles from the terrace surfaces, (i) along the Sakarya River from Boğazköy Village to the industrial site (organized) to calculate average slope for the terraces and (ii) to construct fault perpendicular profiles of the eastern part of the SAS in an attempt to constrain the Late Holocene cumulative vertical offset resolved on the fault.

2.3. Dating

In order to build up the chronology of the Sakarya TSC in the Adapazarı Basin, protocols based on OSL dating were applied to pristine quartz (Aitken, 1998) and k-feldspars (infrared stimulated luminescence, p-IR-IRSL; Thiel et al., 2011). The methodological procedures for the steps of luminescence dating were mineral separation, selection of the protocol, equivalent dose (De) measurements, statistical analysis, and environmental dose rate (Dr) determinations, as detailed thoroughly by Şahiner et al. (2018) and Erturaç et al. (2019). Erturaç et al. (2019) reported 10 luminescence ages covering T3, T2, and T1, which were used in this study, with 2 additional samples (SB-202 A and B) from T4. All of the steps concerning mineral separation wereconducted at the Marmara Luminescence Dating of Terrestrial Archive laboratory (MALTA) of Sakarya University, Research Development and Application Center (SARGEM). Luminescence tests and De measurements from 16 aliquots were performed using a Risø TL/OSL Reader DA-20 (Technical University of Denmark, Center for Nuclear Technologies, Roskilde, Denmark) equipped with $^{90}Sr/^{90}Y$ (0.13 ± 0.04 Gy/s) source installed at the Ankara University Institute of Nuclear Sciences, Luminescence Research and Dating Laboratory. Geochemical analysis of the radioactive elements (U, Th, K, and Rb) was conducted at the accredited ALS-Global Laboratory (Canada), using inductively coupled plasma mass spectroscopy (ICP-MS) for trace elements (ALS Code: ME-MS81) and inductively coupled atomic emission spectroscopy (ICP-AES) for major oxides (ALS Code: ME-ICP06), to determine the environmental Dr. Additionally, to increase the temporal resolution and precision of T2, one in-situ mollusk specimen retrieved from the T2 riser was analyzed by the AMS Laboratory (Poznań, Poland), where sample preparation, measurement of carbon isotopes, and determination the date of the sample was conducted.

3. Results

3.1. Terrace staircases

Figure 3 represents the results of the mapping survey, rtk-GPS profiles, sample/section locations, terrace classification, and distribution within a combined Quaternary geology map showing a 4-step terrace formation in the Adapazarı Basin, complementary to that of Erturaç et al. (2019a). All of these terraces had developed on the Karapürçek Formation. The total destruction of the floodplain (T0) by sand mining over the last 30 years was complied from Okur and Erturaç (2018).

The synthetic profile of the Sakarya TSC in the Adapazarı Basin (Figure 4) represented the relative elevations above the recent flood plain, absolute thickness, geometry, and facies of each terrace step. In Figure 4, the stars indicate the positions of the samples within the terrace section, where blue represents luminescence and black represents the radiocarbon samples. The sections of the terrace steps were measured and classified according to the depositional environment.

3.1.1. Terrace T4 (55 ± 2 m)

To complement to the terrace steps presented by Erturaç et al. (2019), herein, a new terrace step, T4, of the Sakarya TSCs in the Adapazarı Basin, was presented. This terrace is evident, as it forms a wide surface that gently inclined towards the NW. However, the surface is mostly covered with dense vegetation and fine grain debris or mud flows derived from the Karapürçek Formation, and was therefore, very hard to observe. The terrace sediments outcroponly at an isolated section, which stands on the top of a sand-gravel quarry carved inside of the Karapürçek Formation to the east of Boğazköy Village, south of the study area (SB-202, Figures 3, 4, and 5B). This section shows a meter-thick rounded channel of gravel (10–20 cm in diameter) at the bottom and the rest is formed of the horizontal laminated and homogenous fine sand-silt fill of the floodplain. Two samples were collected, with the first from the contact of the channel and the fine-grained layers, and the second taken from topof the floodplain sediments to understand the initiation and end of the depositional period. The measurement of the surface and tread of the terrace revealed that T4 stands at 55 ± 2 m above the recent floodplain (Figure 4).

3.1.2. Terrace T3 (23.7 ± 1 m)

T3 forms stepped morphology, comprising especially wide flats at the western side of the Sakarya River, between Karaçam and Kirazca (Figure 3, SB-24, and SB-06). The erosional contact of the terrace sediments with the basement (Karapürçek Formation) is visible in all of the sections (Figure 4). At section YHT (SB-24), the complete terrace stratigraphy can be observed (Figure 5C). The section starts with large boulders of up to 1 m in diameter, where the main clast lithology comprises limestones and metamorphics. The average grain size of these bedload deposits is 20–30 cm. The grain size continuously fines upward progressively, where the terrace ends with a 1- to 2-m-thick silt-fine sand and silt layer, which is observed

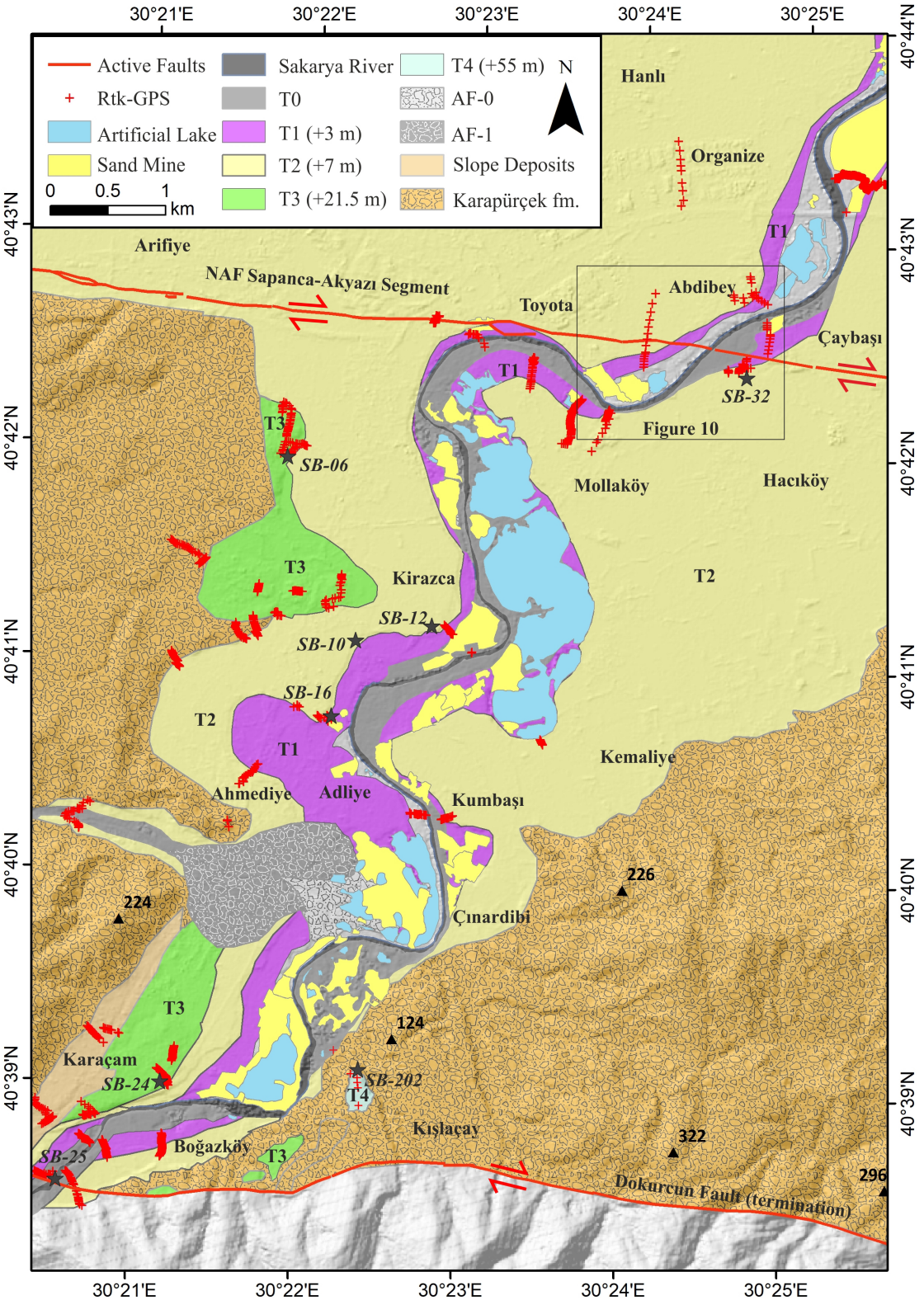

Figure 3. Quaternary geology map of the Adapazarı Basin between Boğazköy-Arifiye (based on Erturaç et al. 2019) including the terrace T4 level and the degree of destruction due to the sand mines (Okur and Erturaç, 2018). Black stars and codes indicate sampling/section locations. Active faults were compiled from Langridge et al. (2002) for SAS and Emre et al. (2018) for the western termination of the Dokurcun Fault.

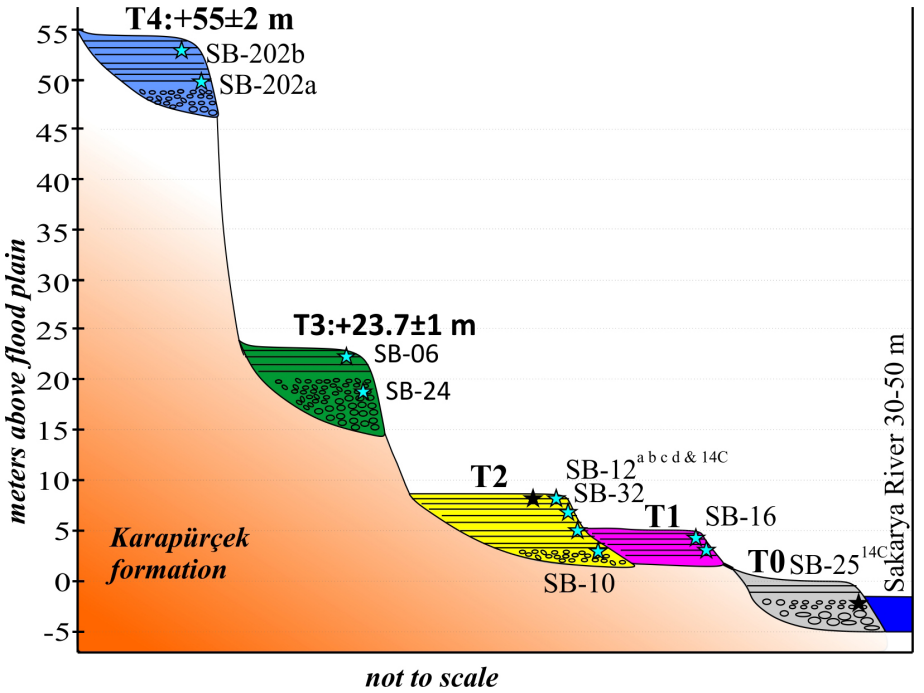

Figure 4. Synthetic profile of the TSCs developed on the Sakarya River at the study area.

to be both homogeneous and intercalated with dark brown, clay rich laminae. The direct contact of T3 with the Karapürçek Formation is visible along the river, enabling the measurement of the channel slope prior to deposition (~1.7‰). The terrace treads were measured as 23.5 (Karaçam) and 23.8 m (Kirazca) with ±1 m error.

3.1.3. Terrace T2 (7–8 m)

This terrace surface forms the wide flat of the Adapazarı Plain, to the south of the NAF (Figure 3). The most representative section of T2 is observed at the SB-12 site, where a total thickness of 4 m is observed (Figure 5D). At the base of this section, the intercalation of 10–20 cm thick layers and lenses of coarse sand and fine pebble showing planar cross beds and horizontal laminated fine-coarse sand layers, is observed through a thickness of 2 m. Up to the section, the intercalation of fine laminated, fine sand, and silt-clay layers,which is observed to be both homogeneous and intercalated with dark brown, clay rich laminae, indicates over bank deposits. The top of the section is silty clay with desiccation cracks and freshwater mollusks deposited during the formation of the floodplain.

3.1.4. Terrace T1

The terrace represents the first phase of the main channel of the modern Sakarya River and is observed as a narrow step in between T2 and T0 that becomes a wider surface to the left bank of the river (Figures 3 and 4). The representative section (SB-16) is 2 m thick and starts with two coarse sand channels showing well-developed cross beds. These channels are separated by laminated silt and fine sand layers. The top of the section is silty clay, showing desiccation cracks formed within the floodplain (Figure 5E).

3.1.5. Terrace T0

The recent floodplain of the Sakarya River (T0) has been almost completely destroyed by intense sand mining (80%), which started in the 1980s and over time, has altered the natural course of the river channel as well (Figure 3, Okur and Erturaç, 2018). The premining era (1975) satellite imagery from the Keyhole optical reconnaissance satellite mission revealed that T0 was formed of by wide (~500 m) point bars of a meandering channel in the study area. The measured amplitude of the channel was 2.4 km, and the sinuosity ratio was 1.5. The uninterrupted T0 surface was measured in a few locations, and barely provided the slope of the floodplain (1.7‰; Figure 6)

3.2. TSC geometry along the river

Precise measurement of the terrace surfaces enabled the calculation of the terrace slopes along the river (Figure 6). Two-point calculation of the slope of the terrace surface and base for T3 indicated that the slope of the Sakarya River channel during the erosional (MIS 4) and the flood plain during the depositional (MIS 3) periods were the same (1.7‰). The linear trend of the surface elevation of T2 surface along the river revealed a lower slope value (1.1‰). T1 and T0 were also observed as distinct surfaces to the south of the SAS, but only confined to the current

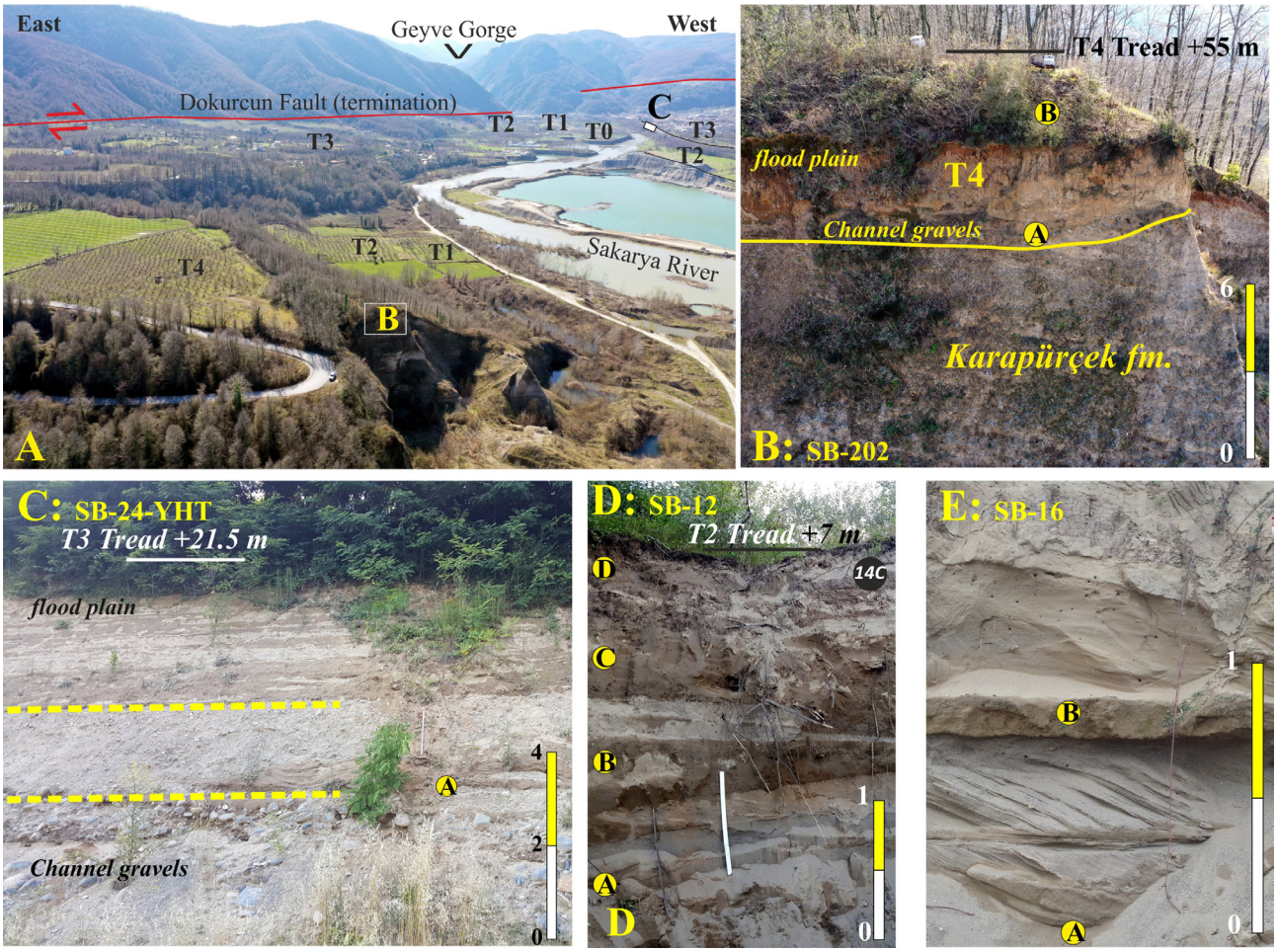

Figure 5. A) Panorama of the Sakarya River valley looking towards the south, and distribution of the TSC. B) Close-up of terrace T4 (SB-202) and OSL sample locations, scale in meters. C) A complete fluvial terrace stratigraphy of terrace T3 at Karaçam-YHT section (SB-24). D) Kirazca section of terrace T2 (SB-12) showing the terrace stratigraphy and also sampling locations including the radiocarbon sample. E) Close-up of the SB-16 section of terrace T1. Yellow and black filled circles indicate sample codes for each section. Scale in meters.

course of the Sakarya River.The slope values calculated for T1 and T0 were 1.2‰ and 1.7‰ respectively. These levels coincided with the T2 surface after a short distance to the north of the SAS (Figure 6). It can be speculated that it is possible that the T1 and T0 levels will not be preserved in the future and will be wiped away during the next (future) erosional period.

3.3. Terrace chronology

Herein, 2 new OSL ages were presented, constraining the depositional period of T4 (55 m) and a single radiocarbon age (SB-12^{14C}) from the uppermost part of T2, complementary to the luminescence and radiocarbon ages for the Sakarya TSC reported by Erturaç et al. (2019) (Table 1). Figure 7details the luminescence signal (I), dose-response curves (II), Tx/Tn graphs (III) for the selected discs and resulting abanico plots, and a combination of the conventional radial plot (IV) and probability density function histogram and scatter plot (V) of the De distribution. The measured disks (16) gave well-resolved, low over-dispersion (OD) De values for samples SB-202-A and SB-202-B (12.3% and 8.9%, respectively) allowing the determination of the equivalent doses with the central age model (Galbraith and Roberts, 2012) at 185 ± 4.6 and 120.6 ± 3.9 Gy, respectively. The environmental Drs of the samples varied due to increase in U and K values, and were calculated as 2.21 and 1.68 Gy/ka (Table 1). All of these determinations resulted in 83.86 ± 2.11 ka for the initiation period and 71.88 ± 2.34 ka for the end of deposition period for T4. Two ages from T3 (SB-24 and SB-06) were reported by Erturaç et al. (2019), constraining the timing of deposition at 41.10 ± 1.83 ka and 30.04 ± 1.06 ka (Table 1).

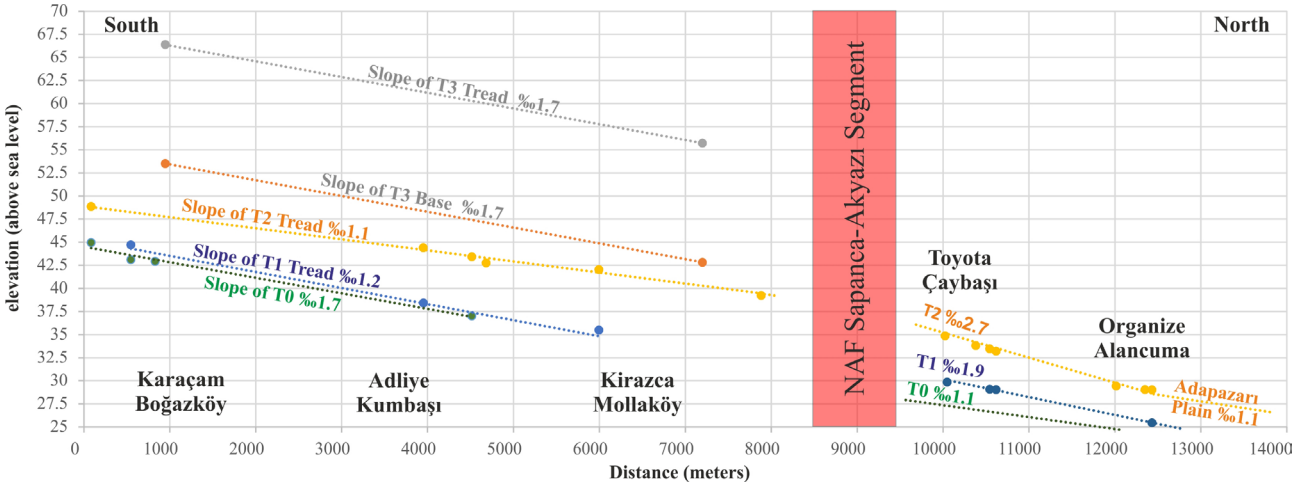

Figure 6. Slope of the Sakarya River flood plain during the late Pleistocene-Holocene using the mean elevation of the terrace surfaces along the river.

The depositional history of the study area for the last 2500 years, with contrast to T2 and T1, was crucial for the scope of this study and is outlined in Figure 8. T2 was previously constrained with 6 luminescence ages (OSL and p-IRIR), indicating continuous deposition between ~9 and 1.8 ka (Table 1, Erturaç et al., 2019a). Within the scope of this study, in order to precisely mark the end of deposition of T2, a new radiocarbon age was obtained from the remains of a single mollusk within the back-swamp deposits from the top of SB-12 section (Figure 6D), which resulted in 1890 ± 30 year/BP. This age was calibrated to calendar ages (BP) with OxCal v.4.4.2 (Ramsey, 2009), using the IntCal20 atmospheric curve (Reimer et al., 2020). Due to the fluctuations in the calibration curve for the time period, the calibrated age yielded a high error rate with 2s (99.7%) determination to 1925–1704 year/calBP (Table 2, Figure 8). This age coincided perfectly with previous OSL dates from the same level (SB-12-D and SB-32, Erturaç et al., 2019a), rectifying the end of the deposition of T2.

The deposition of T1, which was also used as a geomorphic marker in this study, was dated to 1.1–1.06 ka with OSL samples SB-16-A and SB-16-B (Table 1; Erturaç et al., 2019a). After a short erosional period, the recent floodplain (T0) started to develop at 740–648 year/CalBP (Table 2, Figure 8B).

4. Discussion

4.1. Driving mechanisms of fluvial terrace formation

The Sakarya River experienced depositional and erosional periods in response to (i) major and long duration base level changes during the Late Pleistocene and (ii) climate shifts during the Holocene (Erturaç et al., 2019a). These processes resulted in 2 types of terrace formation, stepped (strath) and embedded (fill) terraces (Wegmann and Pazzaglia, 2009). The most possible explanation for the first phenomenon was the Black Sea level changes in response to stadial and interstadial periods during the last Glacial within a specific MIS (Figure 9). In this scenario, the river accumulated during the relative high stands of the Black Sea level during MIS 5a (~84–72 ka), MIS 3 (40–30 ka), and MIS 1 (9 ka–recent), with a calculated average deposition rate of 0.67 mm/year. The erosion occurred during the long low stands of MIS 4 (~72–41 ka) and MIS 2 (~30–9 ka) (Table 1, Figure 9A). The total amount of erosion during these periods was measured as 40 and 20 m (Figure 4) and the incision rates were calculated as 1.3 and 1 mm/year respectively. These erosional periods, accompanied by stable rock uplift, give way to the formation of the stepped terrace morphology reflected in T4 andT3.

During the last glacial period, MIS 5a and the late MIS 3 were marked as depositional periods for major fluvial systems of the southern Black Sea catchment (Erturaç and Güneç Kıyak, 2017; Berndt et al., 2018; Erturaç et al., 2019a). These proposed depositional periods were compatible with previous low-resolution estimations of the Black Sea level, comprising the Tarkhankutian-Karangatian-Tobeckikian (MIS 5) and Surozhian (late MIS 3) high stands or transgressions (Figure 9B, Panin and Popescu, 2007; Yanina, 2014). The high stand during MIS5b to MIS 5a, inferred from T4, was also reflected in the modeled global relative sea level (RSL) curves as ~35 m below sea level (bsl), in between the 2 low stands of MIS 5b and MIS4, which allowed Mediterranean waters to intrude into the Black Sea(Figure 9D, PC1; Spratt and Lisiecki, 2016). The isotope studies of the Sofular Cave records also suggested a marine connection at the time (Figure 9C, Badertscher et al., 2011). In the Sea of Marmara (SoM), ~93–87 ka BP (stadial MIS 5b-c) was defined as a period of

Table 1. Luminescence (OSL and p-IRIR) dates for the Sakarya River TSC. Ages from T1, T2, and T3 were compiled from Erturaç et al. (2019a). Ages marked with * from terrace T4 were reported in this study. De: equivalent dose, OSL: optically stimulated luminescence, P-IRIR: postinfrared-infrared stimulated luminescence, CAM: central age model, FMM: finite mixture model, Drc: cosmic dose rate), Dr: environmental dose rate.

Terrace	*Sample*	*Latitude*	*Longitude*	*Z (m)*	*Depth (cm)*	*Used aliquots*	*Protocol statistical analysis*	*De (Gy)*			*OD (%)*	*U (ppm)*	*Th (ppm)*	*K (ppm)*	*Rb (ppm)*	*H_2O (%)*	*Drc (Gy/ka)*	*Dr (Gray/ka)*			*Luminescence age (ka)*		
T1	SB-16-B	40.68	30.37	35	50	15//16	OSL^{CAM}	2.8	±	0.2	21	1.78	6.8	1.59	60.4	25	0.12	2.37	±	0.01	1.06	±	0.1
T1	SB-16-A	40.69	30.38	35	100	15//16	OSL^{CAM}	3.03	±	0.2	23	1.84	6.52	1.52	58.1	25	0.16	2.35	±	0.01	1.11	±	0.2
T2	SB-32	40.71	30.41	35	50	12//16	OSL^{CAM}	4.35	±	0.2	16	1.8	7.38	1.49	59.3	17	0.15	2.35	±	0.01	1.87	±	0.09
T2	SB-12-D	40.69	30.38	37	20	24//28	OSL^{CAM}	4.22	±	0.41	43	1.76	7.32	1.42	55.4	18	0.18	2.31	±	0.01	1.83	±	0.2
T2	SB-12-C	40.69	30.38	37	50	16	$p\text{-}IRIR^{FMM}$	9.26	±	1	37	1.84	6.52	1.52	58.1	15	0.16	2.48	±	0.02	3.84	±	0.28
T2	SB-12-B	40.69	30.38	37	140	26/28	$p\text{-}IRIR^{FMM}$	9.73	±	0.37	32	1.79	7.4	1.42	51.9	24	0.15	2.42	±	0.03	4.02	±	0.36
T2	SB-12-A	40.69	30.38	37	200	16	$p\text{-}IRIR^{CAM}$	11.6	±	0.6	19	1.74	6.78	1.33	54.9	15	0.21	2.34	±	0.02	4.95	±	0.4
T2	SB-10	40.68	30.38	35	250	16	$p\text{-}IRIR^{CAM}$	19.3	±	0.8	15	1.73	6.51	1.33	48.5	22	0.15	2.14	±	0.01	9.04	±	0.4
T3	SB-06-C	40.7	30.36	60	50	16	OSL^{CAM}	54.6	±	1.9	13	1.58	6.17	1	41.7	29	0.18	1.82	±	0.01	30.04	±	1.06
T3	SB-24-A	40.64	30.34	50	400	16	OSL^{CAM}	83.08	±	3.7	15	1.8	6.47	1.26	54.7	22	0.09	2.04	±	0.01	41.1	±	1.83
*T4**	SB-202B	40.65	30.37	106	50	16	OSL^{CAM}	120.6	±	3.9	12.3	1.33	5.21	1.14	39.5	17	0.17	1.68	±	0.01	71.88	±	2.34
*T4**	SB-202A	40.65	30.37	106	200	15//16	OSL^{CAM}	185	±	4.6	8.9	1.74	6.55	1.52	60.15	14	0.13	2.21	±	0.01	83.86	±	2.11

lacustrine conditions that implied a sea level below the sill depth of the Dardanelles Strait (Çağatay et al., 2019). The overlying sapropel deposition observed in the SoM basins indicated a marine flooding event that connected the Mediterranean to the Black Sea through the shallow straits of the Bosporus and Dardanelles at the time (Çağatay et al., 2019). The late MIS 3 high stand is a matter of debate, the global RSL was estimated as below the Bosporus-Dardanelles threshold (~90 m bsl) (Spratt and Lisiecki, 2016), but was also evidenced in coastal terraces in the Caucasian and Romanian shelf, reflecting that the sea level was 10–40 m bsl (Figure 9D, Panin, 1983; Chepalyga, 1984; Panin and Popescu, 2007) in the Black Sea. However, the $d^{18}O$ composition of the Sofular Cave records (Figure 9C, Badertscher et al., 2011) and paleosalinity interpretations from the Marmara and Black Sea cores (Yanchilina et al., 2019) rejected the idea of the intrusion of marine waters into the freshwater Black Sea at that time period. The most favored explanation for this phenomenon was a possible Caspian-Black Sea connection during the late MIS 3 (Yanina, 2014; Krijgsman et al., 2019), but this still needs to be verified by direct evidence and dating.

The drastic fall of the Black Sea level (~–140 m) during MIS 2 to the Early Holocene (Figure 9D; Ryan et al., 2003; Yanina, 2014; Yanchilina et al., 2017) led to a significant breakthrough for the major rivers of the northwestern Black Sea basin, comprising Dnieper, Dniester, and Danube, causing the formation of canyons with an ~50-m incision of the river valleys (Svitoch et al., 2000). During this period, the amount of vertical incision exceeded 35 m in the main Sakarya River channel in the Karasu Delta (Görür et al., 2001), and the Adapazarı Basin was dissected and the rivers were incised down to 20–30 m (Figure 4; Erturaç et al., 2019a).

The initiation of the last main depositional period in the Sakarya River was directly correlated with the abrupt level rise of the Black Sea, at ~9 ka/BP (Figure 9D; Ryan et al., 2003; Yanchilina et al., 2017), following this long incision period. The Sakarya River responded through the deposition of the second type of terrace, which is embedded (fill terrace) in nature and reflected in T2 (~9–2 ka) and T1-T0(1 ka) (Figures 4, 8, and 9). The humid climatic conditions of the Early-Middle Holocene caused increased discharge of the river (Göktürk et al., 2011), aiding in the refilling of the basin (Figure 4). The last 2000 years of geological history of the Adapazarı Basin is outlined in Figure 8. All hydrological changes leading to erosion and deposition within this time period can be correlated with documented historical climate changes. These historical events are known as the Roman Warm Period, Medieval Dark Ages, Medieval Warm Period, and finally, the Little Ice Age, which were also evidenced in adjacent paleoclimate records (see Erturaç et al., 2019a and the references therein).

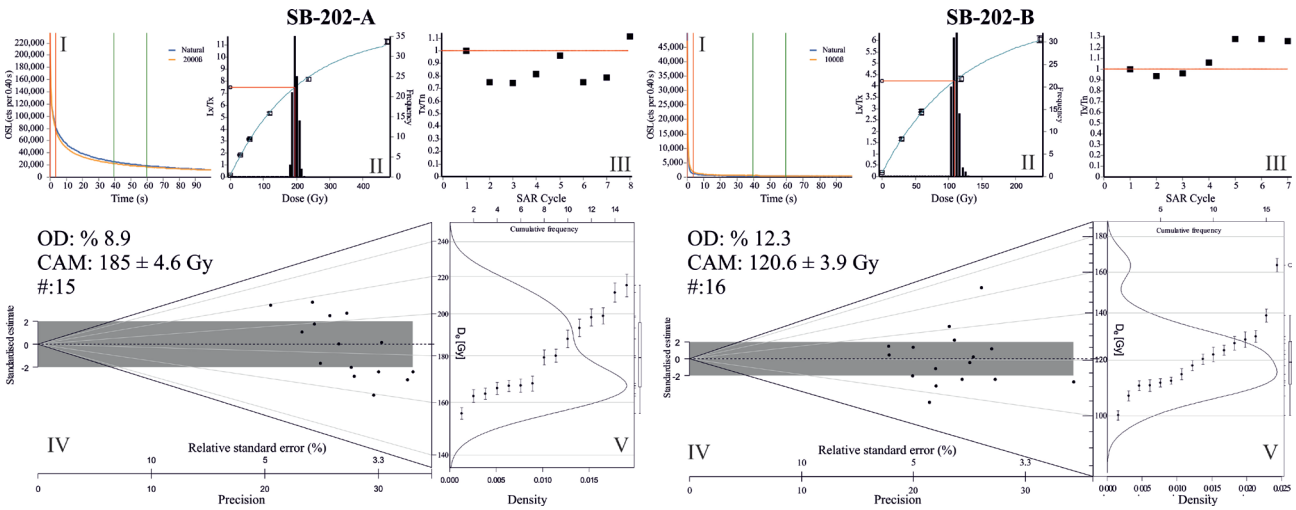

Figure 7. Graphs showing the details of luminescence dating for samples SB-202-A and SB-202-B from terrace step T4. I) Shine-down curves, II) dose response curves, III) Tx/Tn graphs for each SAR cycle, IV) Abanico plots showing both De distributions, and V) scatter plot and kernel density diagrams (see Figure 3 for sampling site, and Figures 4 and 5B for sample positions).

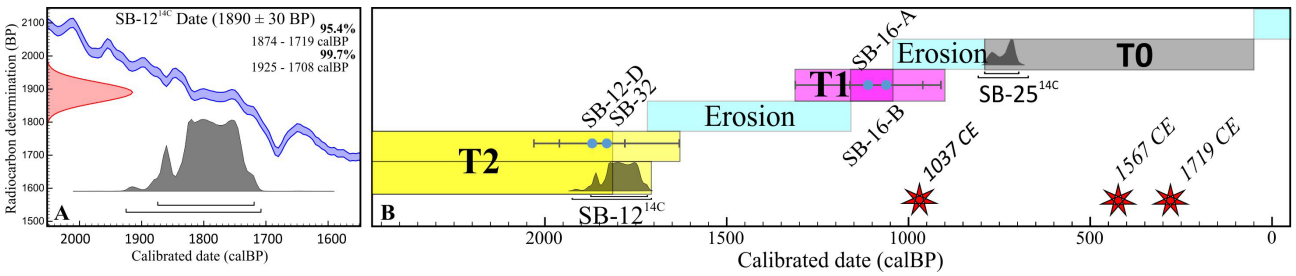

Figure 8. A) Calibration of the SB-12^{14C} radiocarbon date, and B) the geological history of the Adapazarı Basin with respect to the lower terrace steps for the last 2500 years (see Table 1 for references of the dates). Red stars indicate the paleo-earthquakes on the SAS determined by Dikbaş et al. (2018) in the paleoseismic trenches.

Table 2. Radiocarbon ages from the Sakarya River TSC. Age determination from T0 was from Erturaç et al. (2019a); T2 was from this study. All radiocarbon dates were calibrated to calendar ages (BP) with OxCal v.4.4.2 (Ramsey et al., 2009), using the IntCal20 atmospheric curve (Reimer et al., 2020).

Terrace	*Sample*	*Latitude*	*Longitude*	*Z (m)*	*Depth (cm)*	*Age (year/BP)*	*Cal Age (year/BP)*
T0	SB-25^{14C}	40.64	30.34	50	400	760 ± 30	740–648
T2	SB-12^{14C}	40.69	30.38	37	20	1890 ± 30	1925–1704

4.2. Late Pleistocene regional uplift

The distribution of rate and causes of the vertical deformation of Anatolia is a matter of debate and in contrast, there have been relatively few Quaternary geological U_R determinations. The published ages from the marine and fluvial terraces provide a broad look to the variations within the different tectonic zones of the eastern Mediterranean, such as the North Anatolian Shear Zone (NASZ), Pontide Mountain Range-Black Sea Coast (Eurasia), Central Anatolian Plateau, and the Taurus Mountain Range (Anatolia) (Figure 1A). The U_R of the northwestern part of the NASZ is relatively well known. Determinations using U/Th dating of the Middle-Late Pleistocene marine terraces yielded 0.27–0.72 mm/year at Gelibolu and Biga Peninsula (Yaltirak et al., 2002) and an U_R of 0.4–0.46 mm/year for Armutlu Peninsula (Paluska et al., 1989), where the latter was revised to 0.3 mm/year with the new U/Th dates of MIS 5a (~58 ka)

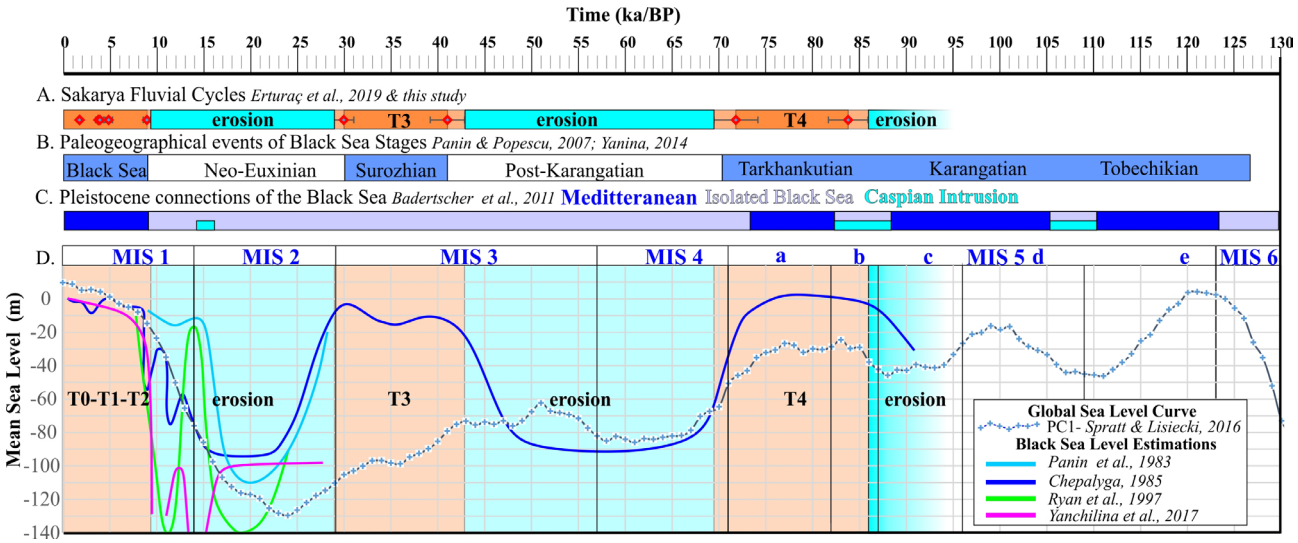

Figure 9. Correlation of the Sakarya River fluvial cycles with the global and Black Sea level changes. A) Depositional and erosional periods with reported luminescence ages and errors for Sakarya River during the late Pleistocene T4 (this study) and T3, Holocene terraces T2, T1 and T0 (Erturaç et al., 2019a). B) Main paleogeographical events of the Black Sea from Panin and Popescu (2007) and Yanina (2014). C) Late Pleistocene connections of the Black Sea inferred from isotope studies (Badertscher et al., 2011). D) late Pleistocene estimations of the global (PC1, Spratt and Lisiecki, 2016) and Black Sea levels (Panin, 1983; Chepalyga, 1984; Ryan et al., 2003; Yanchilina et al., 2017). Boundaries of the marine isotope stages (MIS) after Lisiecki and Raymo (2005).

and MIS 7 (~230 ka) (Yaltırak, 2014), all attributed to compressional bending of the NAF in the region. The U_R of central NASZ was provided from the Yeşilırmak River terraces and determined as 0.94 ± 0.26 mm/year (OSL; Erturaç and Güneç Kıyak 2017). The studies from central-eastern Pontides reported an apparent contrast, where determinations from the coastal dune system (OSL; Yıldırım et al., 2013), coastal terraces (electron spin resonance, ESR; Keskin, et al., 2011), and fluvial terraces (OSL; Berndt et al., 2018) yielded 0.2–0.3 mm/year U_R through the Middle-Late Pleistocene, where the uplift was claimed to be related to large-scale convex bending of the NAF effective for ~100 km to the north (Yıldırım et al., 2011). The long-term average U_R of the central Anatolian plateau was constrained to 0.05–0.06 mm/year from the Kızılırmak River terraces (cosmogenic nuclides, CN; Çiner et al., 2015) and the only determination from western Anatolia was from Kula horst, where the Gediz River terraces yielded 0.16 mm/year (Ar/Ar, Maddy et al., 2017). Further south, the U_R for the central Taurus Mountain Range was determined as 0.6–0.7 mm/year and related with mantle dynamics (CN; Schildgen et al., 2012). From these datasets, it can be concluded that the U_{Rs} within the NASZ were significantly higher than those of central Anatolia, but close to that of the Taurus Mountains.

The contribution herein to the U_R determinations of the Anatolia was provided by utilizing the high terraces (T4 and T3) of the Sakarya River TSCs, which are separated significantly by long duration erosional periods. For calculation of the rate, the positions of the terrace treads (H_S; 55 and 23.65 m) and terrace abandonment ages (T_S; ~72 and ~30 ka) were used, as described in Figure 2. The 3-point average of the calculation (U_R) yielded 0.78 ± 0.06 mm/year, where the standard deviation was 0.014 (Table 3), indicating that the variations of the determined rates were within the measurement errors (s_U) and can be considered as constant during the Late Pleistocene. As detailed previously, therelative position of the T3 surface was determined in 2 locations, which were located 1.5 (23.8 m, Kirazca) and 7 km (23.5 m, Karaçam) to the south of the SAS (Figure 3 and Table 3). The difference of relative elevation of these terrace surfaces (treads) was very small and within the measurement error, and therefore resulted in the same calculated U_{Rs}. This observation indicated that the uplift of the region was uniform, rather than tilting towards to the south. It should also be noted that this long-term uniform uplift determined here was incompatible with the geometry and kinematics of the SAS, where the main motion was pure strike slip (1999a earthquake) with a slight component of transtension (Harvard centroid moment tensor; Ekström et al., 2012). The fault zone also bifurcates into several branches at the study area, which is defined as a transition zone between the strike-slip and extensional regimes of western Anatolia (Figure 1). Aktuğ et al. (2009) attributed a considerable amount of vertical slip, resolved on both the northern and southern segments (SAS and Geyve Fault) of the NAFZ, on their block modeling of the GPS-derived velocity field of western Anatolia.

Table 3. Variables used in the uplift rate determination of the study area. H_S: Hight of terrace surface; Σ_{HS}: measurement error; T_S: age of terrace abandonment; Σ_{TS}: analytical error; U_R: uplift rate; Σ_U: error, STD: standard deviation.

Terrace	H_S (M)	Σ_{HS} (M)	T_S (ka)	Σ_{TS} (ka)	U_R (mm/year)	Σ_U (mm/year)
T4	55	2	71.88	2.34	0.765	0.037
T3 Karaçam	23.8	0.5	30.04	1.06	0.792	0.033
T3 Kirazca	23.5	0.5	30.04	1.06	0.782	0.032
5.1.				Average	0.779	0.034
5.2.				STD	0.014	

Therefore, due to the unique tectonic setting of the region, this value was regarded as the steady rock U_R for the northern slopes of the Samanlıdağ-Kapıdağ Mountain range, bounded by the NAF.

4.3. Horizontal and vertical slip-rate of the Sapanca-Akyazı Segment

The 1999a earthquake (M_w = 7.4) rupture of the NAFmostly follows the T2 surface in the Adapazarı Plain (Barka et al., 2002). The rupture transects the Sakarya River and its Holocene terraces (T2 and T1) between Çaybaşı Village and the Toyota plant (Figure 3; Langridge et al., 2002; Dikbaş et al., 2018). The coseismic horizontal offset was measured as between 310 and 380 cm, with a 15–40-cm vertical component, where the vertical slip of the northern block was attributed to the small step-overs along the segment (Langridge et al., 2002). Along the earthquake rupture, Dikbaş et al. (2018) identified and measured 18.5 ± 0.5 m cumulative offset of the T1 riser at the western bank of the river (yellow X in Figure 10). They determined the age of the terrace with 2 OSL ages to 0.86–0.85 ka, thus constraining the late Holocene slip rate of the SAS to 22 ± 3 mm/year. Erturaç et al. (2019a) determined the age of this terrace as (1.06–1.11 ka) using the same method, but achieving different De and Dr components of the luminescence age formula (Table 1 and Figure 8). Zabcı (2019) recalculated the horizontal slip rate with boxcar-boxcar modeling as 16.7 + 3.6/–2.5 mm/year using the new ages for T1 (Erturaç et al. 2019a).

The high-resolution DSM of the region (Figure 10) shows variations in the elevation of the T2 and T1 surfaces to the south and north of the SAS, which were incompatible with the determined average slope values along the river. Detailed examination of the 2 rtk-GPS and DSM combined topographic profiles, perpendicular to the fault between Çaybaşı and the Toyota plant (Figures 10 and 11), showed vertical variations in the surface elevations of T2 and T1 to the north and south of the fault (Figure 11).

The 1400-m-long Profile 1, from Mollaköy to east of the Toyota plant, passes through the surfaces of T2, the main channel, and T0, T1, and T2 from south to the north (Figure 11 A). The SAS cuts the profile at ~1000 m, deforms the T2 surface, forming an ~1-m visible vertical offset, and also initiates an increased slope. The total elevation difference (ΔSN) of the T2 surface along the profile was measured as 4 m and regarded as an apparent vertical offset of T2 (Figure 11A).

Profile 2, from Çaybaşı to Abdibey, crosses all of the terrace levels and the river channel, and the SAS cuts the profile at 230 m, as observed on the T1 surface (Figure 11B). The apparent offset (ΔSN) of T2 to the south of the fault (right bank of the river) to the north was measured as 4.45 m, where T1 was measured as 2.4 m.

The cumulative vertical slip of the northern part of the fault was calculated by comparing the positions of the lower terraces (T2 and T1) to the south and north of the fault at 2 profiles (ΔSN). The ages regarding the end of deposition of T2 was determined with 2 OSL date (SB-12D and SB-32; Erturaç et al. 2019) and a new radiocarbon date (SB-12^{14C}) (Tables 1 and 2). The SB-16-B OSL date was selected for the age of T1 (Table 1). By comparing the apparent vertical offsets (ΔSN) and the dates(σ_{Ts}), constraining the age of abandonment of the terraces, the average vertical slip rate (V_R) was calculated as 2.27± 0.2 mm/year (Table 3).

However, the Late Pleistocene steady regional rock U_R calculated for the southern block of the fault (0.78 ± 0.03 mm/year) should not be necklaced in this determination. Therefore, this value was used to rectify the position of T2 and T1 to the south of the fault. The uplift corrected (rectified) vertical offset ($\Delta S_{Corr}N$) of T2 was calculated for all 3 age constraints and varied between 2.5 and 3 m. The same calculation was applied to T1 and the offset was constrained as 1.57 m. The uplift corrected vertical offset of T2 and T1 yielded 1.49 ± 0.2 mm/year (STD: 0.04) average V_R (V_RUR_{Corr}) of the focus segment of the SAS for the last 1800 years (Table 4).

This vertical-slip rate resolved on the SAS explained the lack of the T4 and T3 surfaces to the north of the fault and also provided clues on active subsidence of the Adapazarı Plain. If the age of the terraces were related with the calculated V_R, then the position of the former

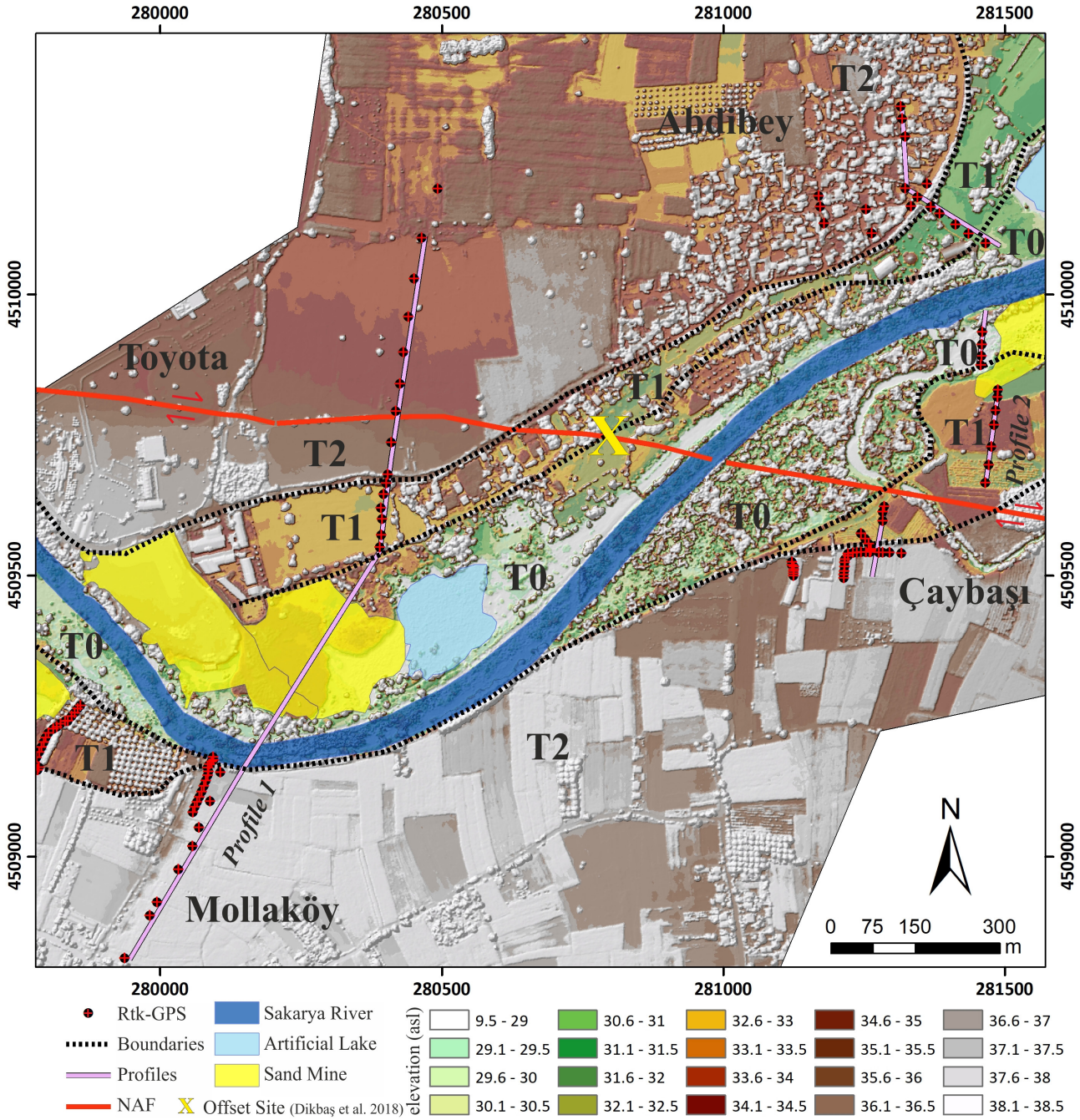

Figure 10. UAV-SfM derived DSM (10 cm) of the focus region of the Sapanca-Arifiye Segment of the 17 August 1999 earthquake rupture.

floodplain surfaces (T4 and T3) can be estimated as 110 ± 10 and 45 ± 5 m, respectively, buried inside of the basin. The geometry and slip resolved on the fault suggested that these surfaces should be inclined slightly to the south.

Based on the inverse modeling of the INSAR data covering the 1999a earthquake, Çakır et al. (2003) proposed that the SAS dipped 85° to the north and the rake of the slip was 175°. This model was supported by GPS-derived postslip motion along the earthquake rupture by Ergintav et al. (2009). Comparing the long-term (~2 ka) horizontal and V_R discussed above, we can attribute 174.7° rake of the slip resolved on the 85° north dipping fault, similar to that in model III of Çakır et al. (2003), fine tuning the 3D geometry of the SAS of the NAF.

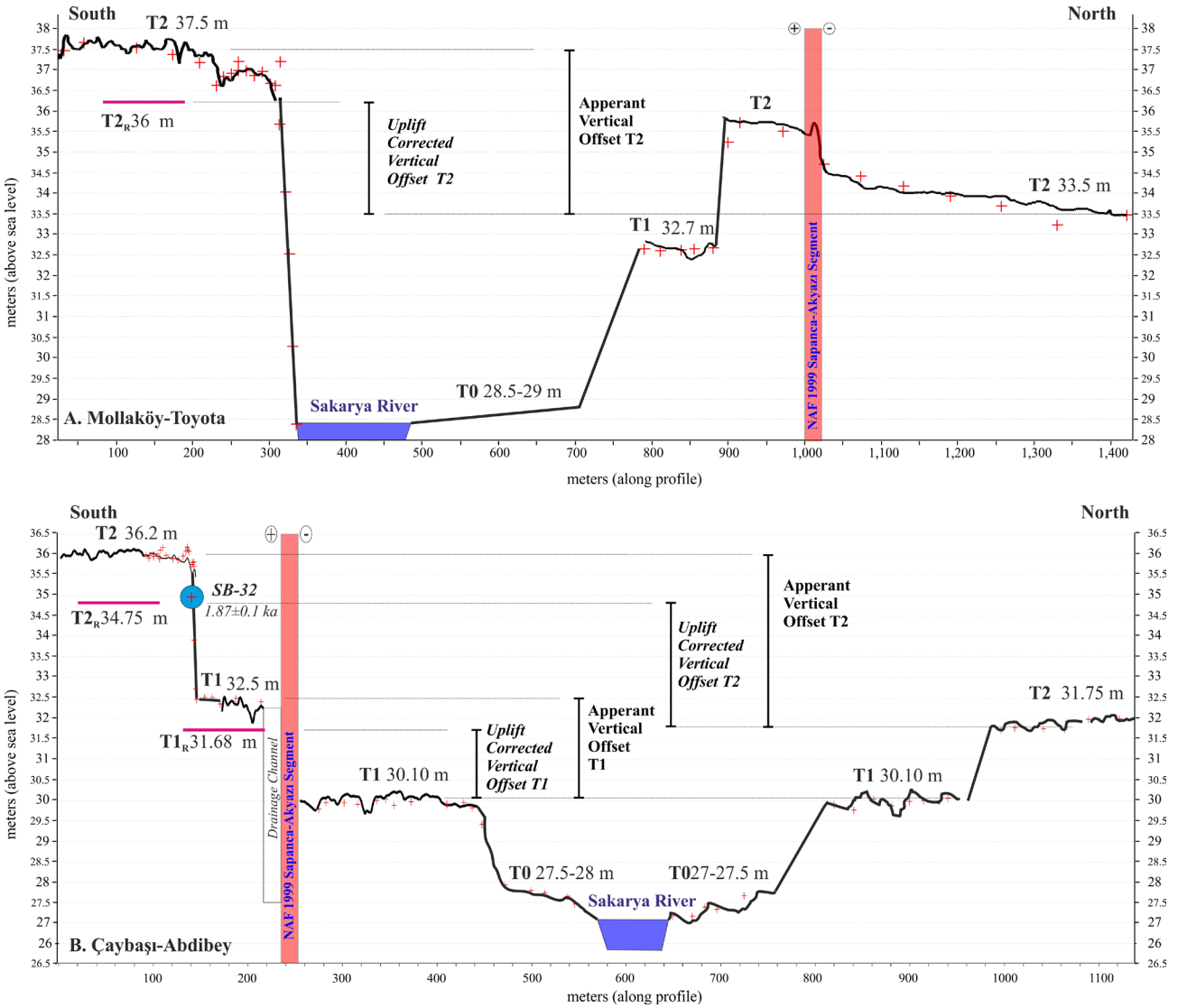

Figure 11. Fault perpendicular microtopographic profiles from A) Mollaköy to the Toyota plant (Profile 1 in Figure 10), and B) Çaybaşı to Abdibey (Profile 2 in Figure 10) showing the vertical offsets of the surfaces of terraces T2 and T1.

4.4. Contribution to the paleoseismic history of SAS

The paleo-earthquakes that ruptured the SAS were determined by Dikbaş et al. (2018). Comparing with the other segments of the 1999 August rupture, it was noticeable that the records covered (Dikbaş et al., 2018) only the historical 1719 CE, 1567 CE, and 1037 CE events within the last 1000 years (Figure 8). The main reason for this gap was probably that during 1.8–1 ka, the Sakarya River was at the state of erosion and there were no depositions on the main channel and the flood plain (Figure 8). The oldest paleoseismic event is evidenced on a trench (EKN, Dikbaş et al., 2018) located at the eastern part of the SAS, at the distal portion of an alluvial fan, covering the deposits of T2.

Comparing the average vertical slip on the SAS during the 1999a earthquake, the cumulative vertical offset of T1 can be accumulated with characteristic slip behavior, producing 460 ± 20 cm horizontal and 40 ± 5 cm vertical slip, similar to the 1999 earthquake (Langridge et al., 2002), in all 4 events that occurred over the last 1000 years. Accordingly, the amount of vertical offset of T2 revealed that there should have been at least 7 earthquakes over the last 1800 years, giving an ~250-year-long term average recurrence period for the segment, which was in agreement with the results for previous determinations for the SAS as well as neighboring segments (Dikbaş et al., 2018). The deposits forming T2 (9–1.8 ka) had recorded almost the entire Holocene activity of the fault

Table 4. Variables used in calculating the V_R for the NAF at the study area. H: Hight of terrace surface, Σ_H: measurement error; H_SUR_{CORR}: uplift corrected height of the southern terrace; ΔSN: elevation difference; $\Delta S_{CORR}N$: uplift corrected elevation difference; T_S: age of terrace abandonment; Σ_{TS}: analytical error; V_R: vertical slip-rate; Σ_{VR}: error; V_RUR_{CORR}: uplift corrected V_R; Σ_{VRCORR}: error for uplift corrected V_R.

Terrace	SITE	H_{SOUTH} (M)	H_SUR_{CORR} (M)	H_{NORTH} (M)	Σ_{HS} (M)	ΔSN (M)	$\Delta S_{CORR}N$ (M)	T_S (ka)	Σ_{TS} (ka)	V_R (mm/yeaR)		Σ_{VR} (mm/yeaR)	V_RUR_{CORR} (mm/yeaR)		Σ_{VRCORR} (mm/year)
T2	Çaybaşı	36.2	34.73	31.75	0.1	4.45	2.98	1.894	0.12	2.35	±	0.16	1.57	±	0.16
T2	Çaybaşı	36.2	34.74	31.75	0.1	4.45	2.99	1.87	0.09	2.38	±	0.13	1.60	±	0.13
T2	Çaybaşı	36.2	34.77	31.75	0.1	4.45	3.02	1.83	0.2	2.43	±	0.27	1.65	±	0.27
T2	Toyota	37.5	36.03	33.5	0.1	4	2.53	1.894	0.2	2.11	±	0.23	1.33	±	0.23
T2	Toyota	37.5	36.04	33.5	0.1	4	2.54	1.87	0.2	2.14	±	0.23	1.36	±	0.23
T2	Toyota	37.5	36.07	33.5	0.1	4	2.57	1.83	0.2	2.19	±	0.25	1.41	±	0.25
T1	Çaybaşı	32.5	31.67	30.1	0.1	2.4	1.57	1.06	0.1	2.26	±	0.23	1.49	±	0.17
								Average:$_{(T2+T1)}$		2.27	±	0.21	1.49	±	0.20
									STD						

and should be further investigated for earthquakes older than 2 ka.

4.5. Implications of the age and total offset of the North Anatolian Fault in the Adapazarı Basin and its initiation time

The extent and geometry of the Karapürçek Formation indicated deposition in a former pull-apart basin controlled by the large step over between the NAFZ Dokurcun and İzmit segments during the Early-Middle Pleistocene (Neugebauer, 1995; Emre et al., 1998; Ünay et al., 2001). At a specific time in the geological evolution of the region, the western part of the Dokurcun Fault in the study area, transferred the strain to the SAS and the rejuvenation of the Adapazarı (Akyazı) Basin was initiated. This change in the tectonic scheme of the region, would have almost instantly terminated the deposition of the Karapürçek Formation, which has now been deeply eroded by the Sakarya River and its parallel river network, all draining into the active depocenter between Akyazı and Arifiye. The exposed sections of the formation also indicated post depositional southwestward tilting of the sedimentary layers at up to 25°, most probably due to the steady uplift of the region (Emre et al., 1998). This evolution model of the formation provided the an opportunity to envisage the timing of the active strand of the NAF (SAS).

The relative position of the highest peak formed on the Karapürçek Formation stands at 330 m above the recent floodplain of the Sakarya River and Adapazarı plain (Figure 12), which stands for the visible thickness of the unit. As an estimation of denudation, 50 m can be added to that. If it is assumed that the calculated U_R in the study area (0.78 ± 0.03 mm/year) was constant through the Middle Pleistocene, the amount of time necessary for the total uplift of the Karapürçek Formation can be estimated (330–380 m) as ~425–490 ka. This age also reflects the timing of the initiation of the SAS and thus, the formation of the Adapazarı Basin.

If the Late Holocene slip rate of the SAS 16.7 + 3.6/–2.5 mm/year (Zabcı, 2019) is compared, one can envisage the total amount of right-lateral offset accommodated on the segment as 7–9 km. This amount of offset was compatible with the length of the Sapanca pull-apart lake and the apparent offset of the Sakarya River between the Geyve-Magara Gorges (Figure 1B).

Accordingly, if the V_R determined in this study was applied to the estimated age, the total thickness of the active depocenter in the Adapazarı Basin (Arifiye-Akyazı) could be calculated as ~665 ± 70 m (Figure 12). If the visible thickness of the Karapürçek Formation (330–380 m) is then added to that, the total Quaternary fill of the Adapazarı Basin reaches to roughly 1100 m, fitting the estimation of Karahan et al. (2001), by seismic profiling. This determination should be refined by detailing the characteristics of the Karapürçek Formation, such as mapping the internal deformation, absolute dating of the termination of the deposition, and also resolving the fading slip rate of the western termination of the Dokurcun Fault after the initiation of the SAS.

Şengör et al. (2005) proposed that the NAFZ evolved from a broad zone of the various types of Riedel shears and folds, towards a single-going (Y shear) fault. They claimed that this transition has been propagating westward since the Middle Miocene in the east and finally reached the SoM as a single throughgoing fault just 200 ka ago, accumulating 4 km cumulative morphological offset (Le Pichon et al., 2001). This model is still under debate, especially concerning the complex fault geometry of the NAFZ within the SoM (Yaltırak et al., 2002; Sorlien et al., 2012; Şengör et al., 2014). Gürbüz and Gürer (2009) claimed that the extinction of the pull-apart basins

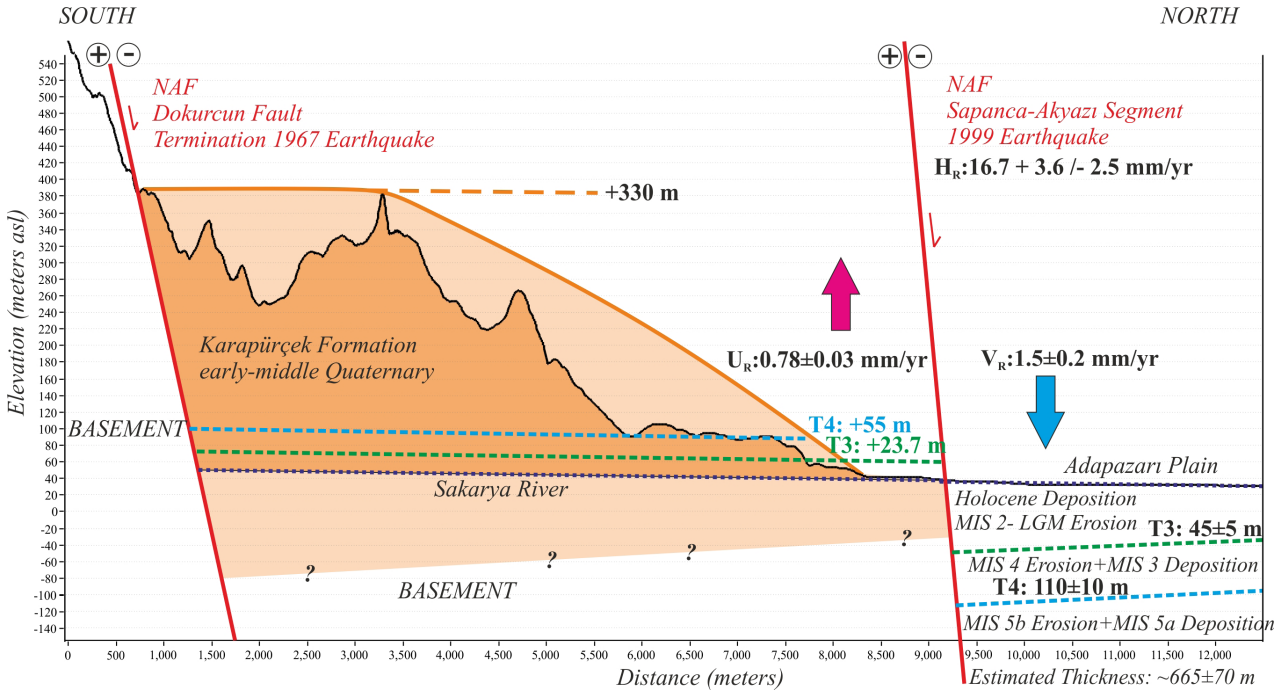

Figure 12. Tectonic interpretation of the S-N topographic profile from the northern slopes of the Samanlı Mountain range, covering the Adapazarı Basin, to estimate the initiation of SAS and the thickness of the Adapazarı Plain.

along the NAFZ occurred almost simultaneously with the Middle Pleistocene (~200 ka). A compilation of limited determinations for the formation of the cross-basin fault branches within the tectonic basins along the NAFZ are shown in Figure 1A. The age determinations were (i) ~200 ka in the SoM (Le Pichon et al., 2001) and (ii) 0.5–0.4 Ma in the Adapazarı Basin in the west (this study). In the central NAFZ, the ages ranged between (iii) 0.9 and 0.7 Ma in the Suluova Basin (Erturaç et al., 2019b) and (iv) 1–0.7 Ma in the Niksar-Erbaa Basin (Barka et al., 2000; Tatar et al., 2007, Erdal et al., 2018). For the eastern most part of the NAFZ, (v) Barka and Gülen (1989) detailed the multiphase evolution of the Erzincan Basin. They claimed that the timing of initiation for the second stage was correlated with volcanism at the basin center (Barka and Gülen, 1989), which was dated to ~1 Ma (Karslı et al., 2008).

The pattern presented herein indicates that the extinction of the pull-apart basins on the NAFZ occurred between 1000 and 200 ka, and the positions/ages resembled a linear migration trend from east to the west.

5. Conclusion

This study on the Late Pleistocene-Holocene TSCs of the Sakarya River in the Adapazarı Basin revealed quantified and relative information on the environmental changes and characteristics of the NAF in the region.

· The terrace formation (cycle) was related with major fluctuations in the Black Sea level during the Late Pleistocene. The initiation of deposition and the abandonment ages of the terraces indicated relative high stands during MIS 5a (~84–72 ka), MIS 3 (40–30 ka), and MIS 1 (since 9 ka). The erosional periods in between the terrace steps reflected the response of the Sakarya River to the relative lowstands.

· The embedded type lower terraces (T2, T1, and T0) have been developing since the last highstand of the Black Sea (Holocene), and responding to the documented and evidenced regional climate changes over the last 2000 years.

· The position and ages of the higher terraces (T4 and T3) were used to calculate the U_R to the south of the NAF. The spatiotemporal position of these terraces yielded an average of 0.78 ± 0.03 mm/year, and uniform and aseismic rock U_R, which was steady through the Late Pleistocene.

· The lower terraces, which were cut and offset by the SAS, revealed 16.7 + 3.6/–2.5 mm/year horizontal (Zabcı, 2019) and 1.49 ± 0.2 mm/year V_R for the last ~1000 (T1) and ~1800 (T2) years, respectively.

· The cumulative horizontal and vertical offset of T1 and the published paleoseismic record indicated the characteristic slip behavior of 4 earthquakes in the last ~1000 years. This determination can be extended to cover T2, yielding an ~250-year late Holocene average earthquake recurrence period for the segment.

The extrapolation of the determined rates through the Middle Pleistocene using the geometry of the Early-Middle Pleistocene Karapürçek Formation, a key clastic

unit, recorded the initiation and rejuvenation of the Adapazarı Basin to the Adapazarı Plain. Hence, the following speculative statements can be made:

· The total amount of time necessary to elevate the Karapürçek Formation to its current position (330–380 m) with the determined U_R in the study area (0.78 ± 0.03 mm/year) can be calculated as 450 ± 50 ka. This estimation also reflects the timing of the initiation of the SAS and thus, the formation of the Adapazarı Plain.

· If the Late Holocene horizontal slip rate of the SAS (16.7 + 3.6/–2.5 mm/year) is extrapolated through the determined age of the fault, the total amount of right-lateral cumulative offset can be calculated as to 7–9 km.

· If the Late Holocene V_R of the SAS (1.5 ± 0.2 mm/year) is extrapolated through the determined age of the fault, the calculation yields the total amount of subsidence in the Adapazarı Plain to 600–750 m and the total thickness of the Adapazarı Basin to ~1100 m.

Acknowledgments

This study was supported by the Scientific and Technological Research Council of Turkey (TÜBİTAK) projects 117Y426 and SAU-BAP 2019-5-20-122, and benefited much from contributions and discussions with Dr's Eren Şahiner, Cengiz Zabcı, Gürsel Sunal, Azad Sağlam-Selçuk, Ali Değer Özbakır, Alper Gürbüz, Aynur Dikbaş, Ökmen Sümer, and MSc Hilal Okur. The author expresses his gratitude to Alper Ulusoy, Seda Çetinle, and Emre Parlakyıldız during field work and dense rtk-GPS and UAV surveys. This study is dedicated to Esen Arpat, Fuat Şaroğlu, and the late Aykut Barka, the pioneers of active tectonic studies in Turkey.

References

Aitken MJ (1998). An Introduction to Optical Dating. The Dating of Quaternary Sediments by the Use of Photon-Stimulated Luminescence. Oxford, UK: Oxford University Press.

Algan O, Gökaşan E, Gazioğlu C, Yücel ZY, Alpar B et al. (2002). A high-resolution seismic study in Sakarya Delta and Submarine Canyon, southern Black Sea shelf. Continental Shelf Research 22 (10): 1511-1527.

Akbayram K, Sorlien CC, Okay A (2016). Evidence for a minimum 52 ± 1 km of total offset along the northern branch of the North Anatolian Fault in northwest Turkey. Tectonophysics 668: 35-41.

Akyuz HS, Hartleb R, Barka A, Altunel E, Sunal G et al. (2002). Surface rupture and slip distribution of the 12 November 1999 Duzce earthquake (M 7.1), North Anatolian fault, Bolu, Turkey. Bulletin of the Seismological Society of America 92 (1): 61-66.

Aktug B, Nocquet JM, Cingöz A, Parsons B, Erkan Y et al. (2009). Deformation of western Turkey from a combination of permanent and campaign GPS data: limits to block-like behavior. Journal of Geophysical Research: Solid Earth 114 (B10). doi: 10.1029/2008JB006000

Armijo R, Meyer B, Hubert A, Barka A (1999). Westward propagation of the North Anatolian fault into the northern Aegean: timing and kinematics. Geology 27 (3): 267-270.

Aslan G, Lasserre C, Cakir Z, Ergintav S, Özarpaci S et al. (2019). Shallow Creep along the 1999 Izmit Earthquake Rupture (Turkey) From GPS and High Temporal Resolution Interferometric Synthetic Aperture Radar Data (2011–2017). Journal of Geophysical Research Solid Earth 124: 2218-2236. doi: 10.1029/2018JB017022

Badertscher S, Fleitmann D, Cheng H, Edwards, RL, Göktürk OM et al. (2011). Pleistocene water intrusions from the Mediterranean and Caspian seas into the Black Sea. Nature Geoscience 4: 236-239. doi: 10.1038/ngeo1106

Barka AA, Gülen L (1989). Complex evolution of the Erzincan Basin (eastern Turkey). Journal of Structural Geology 11: 275-283. doi: 10.1016/0191-8141(89)90067-9

Barka A (1996). Slip distribution along the North Anatolian fault associated with the large earthquakes of the period 1939 to 1967. Bulletin of the Seismological Society of America 86 (5): 1238-1254.

Barka A, Akyüz HS, Cohen HA, Watchorn F (2000). Tectonic evolution of the Niksar and Tasova–Erbaa pull-apart basins, North Anatolian Fault Zone: their significance for the motion of the Anatolian block. Tectonophysics 322 (3-4): 243-264.

Barka A, Akyüz HS, Altunel E, Sunal G, Çakir Z et al. (2002). The surface rupture and slip distribution of the 17 August 1999 İzmit earthquake (M 7.4), North Anatolian fault. Bullettinof Seismological Society of America 92: 43-60. doi: 10.1785/0120000841

Berndt C, Yıldırım C, Çiner A, Strecker MR, Ertunç G et al. (2018). Quaternary uplift of the northern margin of the Central Anatolian Plateau: new OSL dates of fluvial and delta-terrace deposits of the Kızılırmak River, Black Sea coast, Turkey. Quaternary Science Reviews 201: 446-469. doi: 10.1016/j.quascirev.2018.10.029

Bilgin T (1984). Adapazarı Ovası ve Sapanca oluğunun aluviyal morfolojisi ve Kuvaterner'deki Jeomorfolojik tekamülü. İstanbul, Turkey: İstanbul Üniversitesi Edebiyat Fakültesi Matbaası (in Turkish).

Blum MD, Törnqvist TE (2000). Fluvial responses to climate and sea-level change: a review and look forward. Sedimentology 47: 2-48.

Bonnet S, Reimann T, Wallinga J, Lague D, Davy P et al. (2019). Landscape dynamics revealed by luminescence signals of feldspars from fluvial terraces. Scientific Reports 9: 8569. doi: 10.1038/s41598-019-44533-4

Bridgland DR (2000). River terrace systems in north-west Europe: an archive of environmental change, uplift and early human occupation. Quaternary Science Reviews 19: 1293-1303. doi: 10.1016/S0277-3791(99)00095-5

Bridgland DR, Westaway R (2008). Climatically controlled river terrace staircases: a worldwide Quaternary phenomenon. Geomorphology 98: 286-315. doi: 10.1016/j.geomorph.2006.12.032

Bridgland DR, Demir T, Seyrek A, Daoud M, Abou Romieh M et al. (2017). River terrace development in the NE Mediterranean region (Syria and Turkey): patterns in relation to crustal type. Quaternary Science Reviews 166: 307-323. doi: 10.1016/j.quascirev.2016.12.015

Bronk Ramsey C (2009). Bayesian analysis of radiocarbon dates. Radiocarbon 51 (1): 337-360.

Bull WB (2008). Geomorphic Response to Climate Change. Caldwell, NJ, USA: The Blackburn Press.

Chepalyga AL (1984). Inland sea basin. In: Velichko AA, Wright Jr. HE, Barnowsky CW (editors). Late Quaternary Environments of the Soviet Union. Minneapolis, MN, USA: University of Minnesota Press, pp. 229-247.

Çağatay MN, Eriş KK, Makaroğlu Ö, Yakupoğlu N, Henry P et al. (2019). The sea of Marmara during Marine Isotope Stages 5 and 6. Quaternary Science Reviews 220: 124-141. doi: 10.1016/j.quascirev.2019.07.031

Cakir Z, Chabalier JBD, Armijo R, Meyer B, Barka A et al. (2003). Coseismic and early post-seismic slip associated with the 1999 Izmit earthquake (Turkey), from SAR interferometry and tectonic field observations. Geophysical Journal International 155 (1): 93-110.

Cowgill E (2007). Impact of riser reconstructions on estimation of secular variation in rates of strike-slip faulting: revisiting the Cherchen River site along the Altyn Tagh Fault, NW China. Earth Planetary Science Letters 254: 239-255. doi: 10.1016/j.epsl.2006.09.015

Çiner A, Doğan U, Yıldırım C, Akçar N, Ivy-Ochs S et al. (2015). Quaternary uplift rates of the Central Anatolia Plateau, Turkey: insights from cosmogenic isochron-burial nuclide dating of the Kızılırmak River terraces. Quaternary Science Reviews 107: 81-97. doi: 10.1016/j.quascirev.2014.10.007

Dikbaş A, Akyüz HS, Meghraoui M, Ferry M et al. (2018). Paleoseismic history and slip rate along the Sapanca-Akyazı segment of the 1999 İzmit earthquake rupture (Mw = 7.4) of the North Anatolian Fault (Turkey). Tectonophysics 738-739: 92-111. doi: 10.1016/j.tecto.2018.04.019

Doğan A (2004). Sakarya Havzası (Plio-Kuvaterner) güney kesimi Holosen istifinin sedimanter özellikleri ve jeolojik evrimi. MSc, Ankara University, Ankara, Turkey (in Turkish).

Ekström G, Nettles M, Dziewonski AM (2012). The global CMT project 2004-2010: Centroid-moment tensors for 13,017 earthquakes. Physics of the Earth and Planetary Interiors 200-201: 1-9. doi: 10.1016/j.pepi.2012.04.002

Emre Ö, Erkal T, Tchepalyga A, Kazanci N et al. (1998). Neogene-Quaternary evolution of the eastern Marmara Region, Northwest Turkey. Mineral Research Exploration Bulletin 120: 119-145.

Emre Ö, Awata Y, Duman TY (editors.) (2003). 17 Ağustos 1999 İzmit Depremi Yüzey Kırığı (Surface Rupture Associated with the 17 August 1999 İzmit Earthquake). MTA Mineral Research Exploration Special Publications Serie-1: 280. Ankara, Turkey: MTA (in Turkish).

Emre Ö, Duman TY, Özalp S, Şaroğlu F et al. (2018). Active fault database of Turkey. Bulletin of Earthquake Engineering 16 (8): 3229-3275.

Erdal O, Erturaç MK, Dalfes HN, Sen S (2018). Rodents from the Middle Pleistocene of Niksar Basin (Tokat-Turkey): implications on palaeoenvironment and the North Anatolian Fault. Neues Jahrbuch für Geologie und Paläontologie-Abhandlungen 289 (1):77-111. doi: njgpa/2018/0751

Ergintav S, McClusky S, Hearn E, Reilinger R, Cakmak R et al. (2009). Seven years of postseismic deformation following the 1999, M = 7.4 and M = 7.2, İzmit-Düzce, Turkey earthquake sequence. Journal of Geophysical Research: Solid Earth 114 (B7).

Erturaç MK, Güneç Kıyak N (2017). Yeşilırmak taraçalarında (Orta Kuzey Anadolu) geç pleyistosen iklim değişiklikleri ve düşey yönlü deformasyona akarsu cevabının araştırılması. Türkiye Jeoloji Bülteni 60: 615-636 (in Turkish with English abstract). doi: 10.25288/tjb.370625

Erturaç, MK, Şahiner E, Zabcı C, Okur H et al. (2019a). Fluvial response to rising levels of the Black Sea and to climate changes during the Holocene: Luminescence geochronology of the Sakarya terraces. Holocene 29: 941-952. doi: 10.1177/0959683619831428

Erturaç MK, Erdal O, Sunal G, Tüysüz O, Şen Ş (2019b). Quaternary evolution of the Suluova Basin: Implications on tectonics and palaeonvironments of the central North Anatolian Shear Zone. Canadian Journal of Earth Sciences 56 (11): 1239-1261. doi: 10.1139/cjes-2018-0306

Faccenna C, Bellier O, Martinod J, Piromallo C, Regard V (2006). Slab detachment beneath eastern Anatolia: A possible cause for the formation of the North Anatolian fault. Earth and Planetary Science Letters 242 (1-2): 85-97.

Faust D, Wolf D (2017). Interpreting drivers of change in fluvial archives of the Western Mediterranean–a critical view. Earth-Science Reviews 174: 53-83. doi: j.earscirev.2017.09.011

Galbraith RF, Roberts RG (2012). Statistical aspects of equivalent dose and error calculation and display in OSL dating: an overview and some recommendations. Quaternary Geochronology 11: 1-27. doi: 10.1016/j.quageo.2012.04.020

Gedik İ, Aksay A (2002). 1:100 000 ölçekli Türkiye Jeoloji Haritaları, No:32. Adapazarı G-25 paftası. Ankara, Turkey: MTA Jeoloji Etüdleri Dairesi (in Turkish).

Gibbard PL, Lewin J (2009). River incision and terrace formation in the Late Cenozoic of Europe. Tectonophysics 474 (1-2): 41-55.

Gold RD, Cowgill E, Arrowsmith JR, Chen X, Sharp WD et al. (2011). Faulted terrace risers place new constraints on the late Quaternary slip rate for the central Altyn Tagh fault, northwest Tibet. Geological Society of America Bulletin 123 (5-6): 958-978.

Göktürk OM, Fleitmann D, Badertscher S, Cheng H, Edwards RL et al. (2011). Climate on the southern Black Sea coast during the Holocene: Implications from the Sofular Cave record. Quaternary Science Reviews 30: 2433-2445. doi: 10.1016/j.quascirev.2011.05.007

Görür N, Çağatay MN, Emre Ö, Alpar B, Sakınç M et al. (2001). Is the abrupt drowning of the Black Sea shelf at 7150 yr/bp a myth? Marine Geology 176: 65-73. doi: 10.1016/S0025-3227(01)00148-7

Gürbüz A, Gürer ÖF (2008). Tectonic geomorphology of the North Anatolian Fault Zone in the Lake Sapanca basin (eastern Marmara Region, Turkey). Geosciences Journal 12: 215-225. doi: 10.1007/s12303-008-0022-9

Gürbüz, A, Gürer ÖF (2009). Middle Pleistocene extinction process of pull-apart basins along the North Anatolian Fault Zone. Physics of the Earth and Planetary Interiors 173 (1-2): 177-180.

Hussain E, Wright TJ, Walters RJ, Bekaert D, Hooper A et al. (2016). Geodetic observations of postseismic creep in the decade after the 1999 Izmit earthquake, Turkey: implications for a shallow slip deficit. Journal of Geophysical Research Solid Earth 121: 2980-3001. doi: 10.1002/2015JB012737

Jolivet L, Faccenna C, Huet B, Labrousse L, Le Pourhiet L et al. (2013). Aegean tectonics: strain localisation, slab tearing and trench retreat. Tectonophysics 597: 1-33. doi: 10.1016/j.tecto.2012.06.011

Jolivet L, Menant A, Sternai P, Rabillard A, Arbaret L et al. (2015). The geological signature of a slab tear below the Aegean. Tectonophysics 659: 166-182. doi: 10.1016/j.tecto.2015.08.004

Karahan AE, Berckhemer H, Baier B (2001). Crustal structure at the western end of the North Anatolian Fault Zone from deep seismic sounding. Annali di Geofisica 44 (1): 49-68.

Karsli O, Chen B, Uysal I, Aydin F, Wijbrans JR et al. (2008). Elemental and Sr–Nd–Pb isotopic geochemistry of the most recent Quaternary volcanism in the Erzincan Basin, Eastern Turkey: framework for the evaluation of basalt–lower crust interaction. Lithos 106: 55-70.

Keller EA, Pinter N (1996). Active Tectonics: Earthquakes, Uplift, and Landscape. Upper Saddle River, NJ, USA: Prentice Hall.

Keskin S, Pedoja, Bektaş O (2011). Coastal uplift along the eastern Black Sea coast: new marine terrace data from Eastern Pontides, Trabzon (Turkey) and a review. Journal of Coastal Research 27 (6A): 63-73.

Krijgsman W, Tesakov A, Yanina T, Lazarev S, Danukalova G et al. (2019). Quaternary time scales for the Pontocaspian domain: interbasinal connectivity and faunal evolution. Earth-Science Reviews 188: 1-40. doi: 10.1016/j.earscirev.2018.10.013

Lambeck K, Antonioli F, Purcell A, Silenzi S (2004). Sea level change along the Italian coast for the past 10,000 yr: Quaternary Science Reviews 23: 1567-1598. doi: 10.1016/j.quascirev.2004.02.009

Langridge RM, Stenner HD, Fumal TE, Christofferson SA, Rockwell TK et al. (2002). Geometry, slip distribution, and kinematics of surface rupture on the Sakarya fault segment during the 17 August 1999 İzmit, Turkey, earthquake. Bulletin of the Seismological Society of America 92: 107-125. doi: 10.1785/0120000804

Lavé J, Avouac JP (2001). Fluvial incision and tectonic uplift across the Himalayas of Central Nepal. Journal of Geophysical Research 106 (B11): 26561-26591.

Le Pichon X, Şengör AMC, Demirbağ E, Rangin C, Imren C et al. (2001). The active main Marmara fault. Earth and Planetary Science Letters 192 (4): 595-616.

Lisiecki LE, Raymo ME (2005). A Pliocene-Pleistocene stack of 57 globally distributed benthic δ18O records. Paleoceanography 20: PA1003. doi: 10.1029/2004PA001071

Macklin MG, Lewin J, Woodward JC (2012). The fluvial record of climate change. Philosophical Transactions of the Royal Society 370: 2143-2172.

Maddy D, Veldkamp A, Demir T, Van Gorp W, Wijbrans JR et al. (2017). The Gediz River fluvial archive: a benchmark for Quaternary research in Western Anatolia. Quaternary Science Reviews 166: 289-306.

Nasif A, Özel FE, Dondurur D (2020). Seismic identification of gas hydrates: a case study from Sakarya Canyon, western Black Sea. Turkish Journal of Earth Sciences 29: 434-454. doi: 10.3906/yer-1909-2

Neugebauer J (1995). Structures and kinematics of the North Anatolian Fault zone, Adapazarı-Bolu region, northwest Turkey. Tectonophysics 243: 119-134. doi: 10.1016/0040-1951(94)00194-E

Okur H, Erturaç MK (2018). Temporal monitoring of vast sand extraction at Sakarya River floodplain (NW Turkey): implications for environmental impact and natural hazards (Geophysical Research Abstracts 20: EGU2018–847–2). In: EGU General Assembly; Vienna, Austria.

Olszak J (2017). Climatically controlled terrace staircases in uplifting mountainous areas. Global and Planetary Change 156: 13-23.

Öztürk F (1996). Suspended sediment yields of rivers in Turkey. International Association of Hydrological Sciences Publications-Series of Proceedings and Reports 236: 65-72.

Paluska A, Poetsch S, Bargu S (1989). Tectonics, paleoseismic activity and recent deformation mechanism in the Sapanca-Abant region (NW Turkey, North Anatolian Fault Zone). In: Turkish German Earthquake Research Project. Ankara, Turkey: Earthquake Research Institute; Kiel, Germany: University of Kiel. pp. 18-33.

Panin N (1983). Black Sea Coast line changes in the Last 10.000 Years. A new attempt at identifying the Danube mouths as described by the ancients. Dacia. Revue d'Archéologie et d'Histoire Ancienne Bucuresti 27 (1-2): 175-184.

Panin N, Popescu I (2007). The northwestern Black Sea: climatic and sea-level changes in the Late Quaternary. In: Yanko-Hombach V, Gilbert AS, Panin N, Dolukhanov PM (editors). The Black Sea Flood Question: Changes in Coastline, Climate and Human Settlement. New York, NY, USA: Springer, pp. 387-405.

Pazzaglia FJ (2013). Fluvial terraces. In: Shroder JF (editor) Treatise on Geomorphology, Vol. 9-22. San Diego, CA, USA: Academic Press, pp. 379-412.

Philippon M, Brun JP, Gueydan F, Sokoutis D (2014). The interaction between Aegean back-arc extension and Anatolia escape since Middle Miocene. Tectonophysics 631: 176-188. doi: 10.1016/j.tecto.2014.04.039

Reilinger R, McClusky S, Vernant P, Lawrence S, Ergintav S et al. (2006). GPS constraints on continental deformation in the Africa-Arabia-Eurasia continental collision zone and implications for the dynamics of plate interactions. Journal of Geophysical Research: Solid Earth 111 (B5).

Reimer PJ, Austin Wen, Bard E, Bayliss A, Blackwell P et al. (2020). The IntCal20 Northern Hemisphere radiocarbon calibration curve (0–55 kcal BP). Radiocarbon 62: 725-757. doi: 10.1017/RDC.2020.41

Rixhon G, Briant RM, Cordier S, Duval M, Jones A et al. (2017). Revealing the pace of river landscape evolution during the Quaternary: recent developments in numerical dating methods. Quaternary Science Reviews 166: 91-113.

Ryan WB, Major CO, Lericolais G, Goldstein SL (2003). Catastrophic flooding of the Black Sea. Annual Review of Earth and Planetary Sciences 31 (1): 525-554.

Schildgen TF, Cosentino D, Bookhagen B, Niedermann S et al. (2012). Multi-phased uplift of the southern margin of the Central Anatolian plateau, Turkey: a record of tectonic and upper mantle processes. Earth and Planetary Science Letters 317-318: 85-95. doi: 10.1016/j.epsl.2011.12.003

Schumm SA (1993) River response to base level change: Implications for sequence stratigraphy. Journal of Geology 101: 279-294.

Sorlien CC, Akhun SD, Seeber L, Steckler MS, Shillington DJ et al. (2012). Uniform basin growth over the last 500 ka, North Anatolian Fault, Marmara Sea, Turkey. Tectonophysics 518: 1-16.

Spratt RM, Lisiecki LE (2016). A Late Pleistocene sea level stack. Climate of the Past 12: 1079-1092. doi: 10.5194/cp-12-1079-2016

Stein RS, Barka AA, Dieterich JH (1997). Progressive failure on the North Anatolian fault since 1939 by earthquake stress triggering. Geophysical Journal International 128 (3): 594-604.

Sunal G, Erturaç MK(2012). Estimation of the pre-North Anatolian Fault Zone pseudo-paleo-topography: a key to determining the cumulative offset of major post-collisional strike-slip faults. Geomorphology 159: 125-141. doi: 10.1016/j.geomorph.2012.03.013

Sunal G, Erturaç MK, Gutsuz P, Dunkl I, Cakir Z (2019). Reconstructing the deformation of the north Anatolian fault zone through restoring the oligo–miocene exhumation pattern of the almacık block (Northwestern Turkey) based on the apatite (U–Th)/he ages. Canadian Journal of Earth Sciences 56: 1202-1217. doi: 10.1139/cjes-2018-0283

Sümer Ö, Uzel B, Özkaymak Ç, Sözbilir H (2018). Kinematics of the Havran-Balıkesir Fault Zone and its implication on geodynamic evolution of the Southern Marmara Region, NW Anatolia. Geodinamica Acta 30 (1): 306-323.

Svitoch AA, Selivanov AO, Yanina TA (2000). Paleohydrology of the Black Sea Pleistocene Basins. Water Resources 27: 594-603. doi: 10.1023/A:1026661801941

Şahiner E, Erturaç MK, Polymeris GS, Meriç N (2018). Methodological studies on integration time interval's selection for the luminescence ages using quartz and feldspar minerals; sediments collected from Sakarya, Turkey. Radiation Measurements 120: 163-169. doi: 10.1016/j.radmeas.2018.06.024

Şengör AMC, Görür N, Şaroğlu F (1985). Strike-slip faulting and related basin formation in zones of tectonic escape: Turkey as a case study. In: Biddle KT, Christie-Blick N (editors). Strike-slip Deformation, Basin Formation, and Sedimentation. Oklahoma, OK, USA: Society of Economic Paleontologists and Mineralogists, pp. 227-264.

Şengör AMC, Tüysüz O, İmren C, Sakınç M, Eyidoğan H et al. (2005). The North Anatolian Fault: a new look. Annual Reviews of Earth Planetery Sciences 33: 37-112. doi: 10.1146/annurev.earth.32.101802.120415

Şengör, AMC, Grall C, İmren C, Le Pichon X, Görür N et al. (2014). The geometry of the North Anatolian transform fault in the Sea of Marmara and its temporal evolution: implications for the development of intracontinental transform faults. Canadian Journal of Earth Sciences 51 (3): 222-242.

Şengör AMC, Zabcı C, Natal'in BA (2019). Continental transform faults: congruence and incongruence with normal plate kinematics. In: Transform plate boundaries and fracture zones. Amsterdam, Netherlands: Elsevier, pp. 169-247. doi: 10.1016/B978-0-12-812064-4.00009-8

Tari U, Tüysüz O (2016). The effects of the North Anatolian Fault on the geomorphology in the Eastern Marmara Region, Northwestern Turkey. Geodinamica Acta 28: 139-159. doi: 10.1080/09853111.2015.1065308

Tatar O, Yurtmen S, Temiz H, Gürsoy H, Koçbulut F et al. (2007). Intracontinental Quaternary volcanism in the Niksar pull-apart basin, North Anatolian Fault Zone, Turkey. Turkish Journal of Earth Sciences 16 (4): 417-440.

Thiel C, Buylaert J, Murray A, Terhorst B, Hofer I et al. (2011). Luminescence dating of the Stratzing loess profile (Austria)-testing the potential of an elevated temperature post-IR IRSL protocol. Quaternary International 234: 23-31.

Timur E, Aksay A (2002). 1:100 000 ölçekli Türkiye Jeoloji Haritaları, No:31. Adapazarı G-24 paftası. Ankara, Turkey: MTA Jeoloji Etüdleri Dairesi.

Türkeş M (1996). Spatial and temporal analysis of annual rainfall variations in Turkey. International Journal of Climatology 16: 1057-1076.

Ünay E, Emre Ö, Erkal T, Keçer M (2001). The rodent fauna from the Adapazarı pull-apart basin (nwanatolia): its bearings on the age of the north anatolian fault. Geodinamica Acta 14: 169-175. doi: 10.1080/09853111.2001.11432442

Vandenberghe J (2002). The relation between climate and river processes, landforms and deposits during the Quaternary. Quaternary International 91: 17-23.

Vandenberghe J (2003). Climate forcing of fluvial system development: an evolution of ideas. Quaternary Science Reviews 22: 2053-2060.

Wallinga J (2002). Optically stimulated luminescence dating of fluvial deposits: a review. Boreas 31: 303-322.

Wegmann KW, Pazzaglia FJ (2009). Late Quaternary fluvial terraces of the Romagna and Marche Apennines, Italy: climatic, lithologic, and tectonic controls on terrace genesis in an active orogen. Quaternary Science Reviews 28: 137-165. doi: 10.1016/j.quascirev.2008.10.006

Westaway R (2012). A numerical modelling technique that can account for alternations of uplift and subsidence revealed by Late Cenozoic fluvial sequences. Geomorphology 165: 124-143.

Yaltırak C (2002). Tectonic evolution of the Marmara Sea and its surroundings. Marine Geology 190: 493-529.

Yaltirak C, Sakinç M, Aksu AE, Hiscott RN, Galleb B et al. (2002). Late Pleistocene uplift history along the southwestern Marmara Sea determined from raised coastal deposits and global sea-level variations. Marine Geology 190: 283-305.

Yaltırak C, Aksu AE, Hiscott RN (2014). Late Pleistocene uplift history along the Eastern Marmara Sea (Northern Armutlu Peninsula) determined from raised coastal deposits and global sea-level variations. In: Implications of Late Quaternary Sea Level Changes on the Eastern Mediterranean and Black Sea Coasts, International Workshop in the framework of Turkish-German Science Year 2013–2014; İstanbul, Turkey.

Yanchilina AG, Ryan WBF, McManus JF, Dimitrov P, Dimitrov D et al. (2017). Compilation of geophysical, geochronological, and geochemical evidence indicates a rapid Mediterranean-derived submergence of the Black Sea's shelf and subsequent substantial salinification in the early Holocene. Marine Geology 383: 14-34. doi: 10.1016/j.margeo.2016.11.001

Yanchilina AG, Grall C, Ryan WBF, McManus JF, Major CO (2019). Lack of marine entry into Marmara and Black Sea-lakes indicate low relative sea level during MIS 3 in the northeastern Mediterranean. Climate of the Past Discussions. doi: 10.5194/cp-2019-30

Yanina TA (2014). The Ponto-Caspian region: environmental consequences of climate change during the Late Pleistocene. Quaternary International 345: 88-99. doi: 10.1016/j.quaint.2014.01.045

Yıldırım C, Schildgen TF, Echtler H, Melnick D, Strecker MR (2011). Late Neogene and active orogenic uplift in the central Pontides associated with the north Anatolian Fault: implications for the northern margin of the central Anatolia plateau, Turkey. Tectonics 30: TC5005.

Yıldırım C, Melnick D, Ballato P, Schildgen TF, Echtler H et al. (2013). Differential uplift along the northern margin of the Central Anatolia Plateau: inferences from marine terraces. Quaternary Science Reviews 81: 12-28.

Yigitbaş E, Elmas A, Sefunç A, Özer N (2004). Major neotectonic features of eastern Marmara region, Turkey: Development of the Adapazari-Karasu corridor and its tectonic significance. Geological Journal 39: 179-198. doi: 10.1002/gj.962

Zabcı C (2019). Spatio-temporal behaviour of continental transform faults: Implications from the late quaternary slip history of the North Anatolian Fault, Turkey. Canadian Journal of Earth Sciences 56: 1218-1238. doi: 10.1139/cjes-2018-0308

Zhang JY, Liu-Zeng J, Scherler D, Yin A, Wang et al. (2018). Erratum: Spatiotemporal variation of late Quaternary river incision rates in southeast Tibet, constrained by dating fluvial terraces. Lithosphere 10: 676-676. doi: 10.1130/L686E.1